



# Modeling deformation and failure of viscoelastic composites at finite strains

Jacob Aboudi<sup>1</sup> · Konstantin Y. Volokh<sup>2</sup>

Received: 19 May 2020 / Accepted: 17 August 2020  
© Springer Nature Switzerland AG 2020

## Abstract

A micromechanical analysis is proposed for the establishment of the macroscopic constitutive relations for viscoelastic composite materials undergoing large deformations. The composites are assumed to possess a triply periodic microstructure and their viscoelastic constituents are modeled by the incorporation of the viscoelastic effects with an arbitrary chosen hyperelastic strain energy function. Furthermore, an energy limiter is introduced which enforces the saturation of the viscoelastic strain energy function. The value of the strain energy at the saturation corresponds to the failure energy of the viscoelastic constituent. In conjunction with the derived micromechanical analysis, the occurrence of the energy saturation of the viscoelastic constituent predicts the composite failure. Applications are given for the determination of the macroscopic (overall) response and creep of a viscoelastic unidirectional composite, and the behavior of viscoelastic porous materials. In all cases, failure occurrences of the unidirectional composite and porous materials are predicted.

**Keywords** Finite viscoelasticity · Strain energy limiters · Failure · Softening · Composite materials · Porous materials · Micromechanics · High-fidelity generalized method of cells

## 1 Introduction

Materials can exhibit time-dependent behavior such as creep under constant stress, relaxation under constant deformation, and the dependence of their response to different rates of applied loading. These viscoelastic effects can be modeled in the framework of infinitesimal or finite strain theories. For the latter theory, see the monographs by [8, 10, 13] and [21], for example.

There are several approaches for the incorporation of viscoelastic effects in the constitutive equations of elasticity at finite strain; see [7] for a list of references and for these authors' approach to model viscoelasticity at high rates. In the present investigation, the three-dimensional finite viscoelastic constitutive relations that were presented by [14] are adopted. This model, which is motivated by the linear theory of viscoelasticity, is based on an appropriately chosen hyperelastic strain energy function. It is very general since the convolution integral that appears in the equations may involve several relaxation times, a continuous spectrum of relaxation times or fractional derivatives. The resulting constitutive relations recover this strain energy of finite elasticity for a very fast or very slow process.

The various strain energy functions that have been developed describe the behavior of isotropic hyperelastic materials subjected to large deformations do not predict failure. The stresses which are derived from these strain energy functions increase monotonously as the applied deformations increase. This behavior is not realistic since a real material cannot sustain

---

✉ Jacob Aboudi  
aboudi@eng.tau.ac.il

Konstantin Y. Volokh  
cvolokh@technion.ac.il

<sup>1</sup> Faculty of Engineering, Tel Aviv University, Ramat Aviv 69978, Israel

<sup>2</sup> Faculty of Civil Engineering, Technion-Israel Institute of Technology, Haifa 32000, Israel

large amount of strain energy and deformation without failure. Consequently, in a series of publications, the concept of an energy limiter has been introduced to enforce saturation of the strain energy (see [19] and [21] for example and references cited there). The energy limiter which bounds the amount of strain energy that can be accumulated during deformation is incorporated with the constitutive relation itself which has been designated for the description of the material response. As a result, an enhanced finite strain constitutive equation is obtained which provides the critical (saturation) value of the strain energy function at which failure of the material occurs and at which its static stability is lost. In addition, it has been shown that the critical values of the modified strain energy function form a good indicator of the failure of the material when it is subjected to a combined loading. This has been shown by [17] and [18] for the two types of rubber and for a biological tissue, respectively. It turns out that this critical value is advantageous over other failure criteria such as the critical stretch, stress, shear stress, or von Mises; see [17] for a detailed discussion. In a recent publication, [7] extended the incorporation of the energy limiters with hyperelastic strain energy functions to viscoelastic constitutive equations for the modeling of failure of elastomers at high strain rates.

Composite materials can be formed by reinforcing a soft matrix by high modulus fibers. Tires form an example of layered multi-component structures that consist of rubbery matrices and stiff reinforcements made of steel wires or synthetic fibers. The high-modulus, low-elongation cords carry most of the load, and the low-modulus, high-elongation rubber matrix preserves the integrity of the composite and transfers the load. The primary objective of this type of composite is to withstand large deformation and fatigue loading while providing high load carrying capacity. Another example is the myocardium which is the middle layer in the heart wall, which consists of parallel muscle fibers that are organized into sheets, thus forming an orthotropic laminated structure with a transversely isotropic behavior in each lamina (see [11] and [5] for further discussion).

Micromechanical analyses form a convenient and effective approach for the establishment of constitutive equations which are capable of the prediction of the global (macroscopic) behavior of composite materials undergoing large deformation. These micromechanical analyses of composites which are composed of isotropic constituents are advantageous over macromechanics approaches which propose in advance an anisotropic strain energy function which models the behavior of the composite. The determination of the material parameters and the specific functional form of the strain energy function dependence on the invariants in these anisotropic strain energy functions may be a formidable task unless some assumptions are made.

The high-fidelity generalized method of cells (HFGMC) is a micromechanical theory that is based on the homogenization technique of periodic composites. This micromechanical analysis is capable of establishing the finite strain macroscopic constitutive relations of composites which consist of various types of hyperelastic, viscoelastic, and inelastic constituents; see Chapter 9 of [5] where the reliability and accuracy of its prediction are extensively examined and verified together with various applications. As shown, the micromechanical analysis relies on the tangential formulation of each constituent of the composite, according to which the stress increments are expressed in terms of the deformation gradient increments via the instantaneous tangent tensor of the phase. The micromechanical analysis establishes the effective instantaneous tangent tensor of the composite which relates the average stress increments to the average deformation gradient increments.

The HFGMC has been employed by [3] for the prediction of the behavior of viscoelastic composites at finite strains in which the specific viscoelastic modeling of the phase is referred to as finite viscoelasticity theory. Micromechanical analyses of thermo-viscoelastic composites are given by [1] and [4]. In both [3] and [4], damage effects on the material response are taken into account by incorporating equations that describe the rate of damage evolution. It should be emphasized here that whereas in the framework of the continuum damage mechanics the damage variables form additional internal variables, the strain energy limiter approach does not use internal variables.

In [6], the HFGMC was employed for the failure prediction of unidirectional elastic composites undergoing large deformations. To that end, the hyperelastic strain energies of numerous soft materials were enhanced by the incorporation of strain energy limiters. These materials form the type of a soft matrix which is reinforced by stiff fibers thus forming a composite. The resulting composites were analyzed by the HFGMC micromechanics which was employed to establish the global behavior of the considered multiphase materials. In particular, it was possible to predict the values of the failure stress and deformation of the composites.

In the present investigation, the failure prediction of triply periodic viscoelastic composites undergoing large deformations is presented. Thus, the offered analysis is capable of modeling continuous reinforced viscoelastic composites as well as porous viscoelastic materials. The composite consists of a soft viscoelastic matrix whose constitutive relations are based on the model of [14]. The reinforcing fibers are represented by a hyperelastic strain energy function (although the HFGMC analysis is capable of considering viscoelastic fibers as well). The global (macroscopic) constitutive equations of the viscoelastic composite are established and the failure of the composite is determined by the failure of its soft viscoelastic

matrix. Applications are given for a unidirectional fiber-reinforced composite subjected to various types of loading which are applied at various rates, porous viscoelastic materials, and creep of the unidirectional composites under transverse and biaxial stress loading. Comparisons with the corresponding behavior of elastic composites in which the viscoelastic effects are neglected are shown.

The present article is organized as follows. In Section 2, the constitutive viscoelastic modeling of the monolithic material at finite strains is described together with the incorporation of the strain energy limiter. Next, the tangential formulation of these constitutive relations is established. In Section 4, the HFGMC micromechanical analysis is derived from which the instantaneous concentration, stiffness, and viscoelastic tensors are established. In Section 5, applications are given for a viscoelastic monolithic material, unidirectional composite, and porous material. Finally, the creep of a viscoelastic unidirectional composite is investigated. The article is finalized by a ‘‘Conclusion’’ section.

## 2 Constitutive and governing equations of finite strain viscoelastic materials

Let  $\mathbf{F}$  denote the deformation gradient tensor with the corresponding Green-Lagrange strain tensor  $\mathbf{E} = (\mathbf{F}^T \mathbf{F} - \mathbf{I})/2$ . The strain energy functional of the viscoelastic material is taken as:

$$W(\mathbf{E}, \mathbf{H}^{(n)}) = W^\infty(\mathbf{E}) + \sum_{n=1}^N \mathbf{H}^{(n)} : \mathbf{E} \tag{1}$$

where  $W^\infty$  is the elastic strain energy for long-term (equilibrium) deformations, and  $\mathbf{H}^{(n)}$  is a set of  $N$  stress-like internal variables. The following expression for the second Piola-Kirchhoff stress tensor is obtained.

$$\mathbf{S} = \frac{\partial W^\infty(\mathbf{E})}{\partial \mathbf{E}} + \sum_{n=1}^N \mathbf{H}^{(n)} \tag{2}$$

Since the long-term contribution at equilibrium can be related to the short-term (initial) one, it can be concluded that this model is based on the additive split of the stress tensor into equilibrium and nonequilibrium parts.

Motivated by the similarity of the representation that is expressed by Eq. 2 and the equations of small strain viscoelasticity that correspond to the generalized Maxwell model, the internal variables  $\mathbf{H}^{(n)}$  at time  $t$  can be expressed in terms of convolution integrals [14]:

$$\mathbf{H}^{(n)}(t) = \int_0^t \dot{\mathbf{S}}^{(n)}(\tau) \exp\left(-\frac{t-\tau}{\tau_n}\right) d\tau, \quad n = 1, \dots, N \tag{3}$$

where  $\mathbf{S}^{(n)}$  are internal stresses obtained from the strain energy functions  $W^{(n)}$  as follows:

$$\mathbf{S}^{(n)} = \frac{\partial W^{(n)}}{\partial \mathbf{E}} \tag{4}$$

$\tau_n$  are relaxation times and the dot denotes the material time derivative.

The initial (short-term) elastic strain energy at  $t = 0$ ,  $W^{(0)}$ , is given by:

$$W^{(0)} = W^\infty + \sum_{n=1}^N W^{(n)} \tag{5}$$

Next, the following simplification is introduced. It is assumed that each term  $W^{(n)}$  is just a scalar multiplier of  $W^{(0)}$ , namely  $W^{(n)} = \delta_n W^{(0)}$ . Consequently,

$$W^\infty = W^{(0)} \left[1 - \sum_{n=1}^N \delta_n\right] \tag{6}$$

Thus,

$$W = W^{(0)} \left(1 - \sum_{n=1}^N \delta_n\right) + \sum_{n=1}^N \mathbf{H}^{(n)} : \mathbf{E} \tag{7}$$

and

$$\mathbf{S}(t) = \left(1 - \sum_{n=1}^N \delta_n\right) \frac{\partial W^{(0)}}{\partial \mathbf{E}} + \sum_{n=1}^N \mathbf{H}^{(n)}(t) \quad (8)$$

with

$$\mathbf{H}^{(n)}(t) = \delta_n \int_0^t \dot{\mathbf{S}}^{(0)}(\tau) \exp\left(-\frac{t-\tau}{\tau_n}\right) d\tau \quad (9)$$

with  $\mathbf{S}^{(0)} = \partial W^{(0)} / \partial \mathbf{E}$ . Relations (8) and (9) form the constitutive equations of the monolithic viscoelastic material.

As the applied deformation on the material increases, both the elastic strain energy and the corresponding stress increase as well. Theoretically, there is no limit to the increase of these quantities which obviously is not a realistic situation. In order to limit the ability of the material to accumulate strain energy during deformation, [20] introduced the concept of energy limiter. According to this concept, the elastic strain energy is replaced by a new strain energy function  $\psi$  such that:

$$\psi = \psi^F - \psi^E(\mathbf{C}), \quad \mathbf{C} = \mathbf{F}^T \mathbf{F}, \quad \mathbf{E} = \frac{1}{2}(\mathbf{C} - \mathbf{I}) \quad (10)$$

where  $\psi^F$  and  $\psi^E(\mathbf{C})$  denote the failure and elastic energies, respectively. The failure energy (energy of full separation) is given by:

$$\psi^F = \frac{\phi}{m} \Gamma\left(\frac{1}{m}, 0\right) \quad (11)$$

The elastic strain energy is defined by:

$$\psi^E(\mathbf{C}) = \frac{\phi}{m} \Gamma\left(\frac{1}{m}, \frac{W^m}{\phi^m}\right) \quad (12)$$

where  $W$  is the elastic strain energy of the undamaged material and  $\phi$ ,  $m$  are material parameters. In these equations,  $\Gamma(s, x)$  is the upper incomplete gamma function defined by:

$$\Gamma(s, x) = \int_x^\infty t^{s-1} \exp(-t) dt \quad (13)$$

It is assumed that elasticity, i.e., solid-like behavior, is defined by the molecular bonds, while viscosity, i.e., fluid-like behavior, is defined by the internal friction. Hence, failure of the viscoelastic material is achieved by limiting the equilibrium (long term) energy growth  $W^\infty$ . The stress tensor  $\mathbf{S}$  is determined from Eqs. 10 and 8 yielding:

$$\begin{aligned} \mathbf{S}(t) &= \frac{\partial \psi}{\partial \mathbf{E}} + \sum_{n=1}^N \mathbf{H}^{(n)}(t) \\ &= \frac{\partial \psi}{\partial W^\infty} \frac{\partial W^\infty}{\partial \mathbf{E}} + \sum_{n=1}^N \mathbf{H}^{(n)}(t) \end{aligned} \quad (14)$$

Since

$$\frac{\partial \psi}{\partial W^\infty} = \exp\left[-\left(\frac{W^\infty}{\phi}\right)^m\right] \quad (15)$$

it follows that

$$\mathbf{S}(t) = \exp\left[-\left(\frac{W^\infty}{\phi}\right)^m\right] \frac{\partial W^\infty}{\partial \mathbf{E}} + \sum_{n=1}^N \mathbf{H}^{(n)}(t) \quad (16)$$

According to Eq. (6),  $W^\infty$  can be expressed in terms of  $W^{(0)}$ , hence:

$$\mathbf{S}(t) = \exp\left[-\left(\frac{W^\infty}{\phi}\right)^m\right] \left[1 - \sum_{n=1}^N \delta_n\right] \mathbf{S}^{(0)} + \sum_{n=1}^N \mathbf{H}^{(n)}(t) \quad (17)$$

In the case when the effect of the strain energy limiter is canceled,  $\phi \rightarrow \infty$ , and Eq. 16 reduces to Eq. 8 or 2.

In conclusion, the finite strain viscoelastic material is characterized by its short-term hyperelastic strain energy function  $W^{(0)}$  (e.g., Mooney-Rivlin expressed either in terms of the invariants of  $\mathbf{C}$  or in terms of the principal stretches), the relaxation times  $\tau_n$ , coefficients  $\delta_n$ , and the strain energy limiter parameters  $\phi$  and  $m$ .

### 3 The constitutive tangential formulation

The hyperelastic isotropic strain energy function  $W^{(0)}$  is usually expressed in terms of the invariants  $I_1, I_2$  and  $I_3$  of  $\mathbf{C}$ :

$$I_1 = tr(\mathbf{C}), \quad I_2 = \frac{1}{2} (tr^2(\mathbf{C}) - tr(\mathbf{C}^2)), \quad I_3 = det(\mathbf{C}) \tag{18}$$

Thus, (4) with  $n = 0$  yields after some manipulations that the increments of  $\mathbf{S}^{(0)}$  and  $\mathbf{C}$  are related by:

$$\Delta \mathbf{S}^{(0)} = \frac{1}{2} \mathbf{D}^{(0)} : \Delta \mathbf{C} \tag{19}$$

where the the 4th-order tangent tensor  $\mathbf{D}^{(0)}$  is given by:

$$\mathbf{D}^{(0)} = 4 \frac{\partial^2 W^{(0)}}{\partial \mathbf{C} \partial \mathbf{C}} \tag{20}$$

It can be shown, [16], that the following approximation can be established for the internal variables  $\mathbf{H}^{(n)}$  at time  $t$ :

$$\mathbf{H}^{(n)}(t) = \delta_n \frac{\Delta \mathbf{S}^{(0)}}{\Delta t} \tau_n \left[ 1 - \exp\left(-\frac{\Delta t}{\tau_n}\right) \right] + \exp\left(-\frac{\Delta t}{\tau_n}\right) \mathbf{H}^{(n)}(t - \Delta t) \tag{21}$$

where  $\Delta t$  is a small time increment. Thus, the following expression for the increment of  $\mathbf{H}^{(n)}(t)$  can be obtained:

$$\Delta \mathbf{H}^{(n)}(t) = \beta_n \delta_n \Delta \mathbf{S}^{(0)}(t) - \alpha_n \mathbf{H}^{(n)}(t - \Delta t) \tag{22}$$

where  $\alpha_n = 1 - \exp(-\frac{\Delta t}{\tau_n})$ ,  $\beta_n = \alpha_n \tau_n / \Delta t$ . This recursive relation is used to update the internal variables at every increment.

In conjunction with Eq. 22, the increment of the second Piola-Kirchhoff stress tensor  $\mathbf{S}$  can be determined from Eq. 17 as follows:

$$\begin{aligned} \Delta \mathbf{S}(t) = & \eta \left[ \Delta \mathbf{S}^{(0)}(t) - \frac{m}{\phi^m} (W^\infty)^{m-1} \mathbf{S}^{(0)}(t) \Delta W^\infty \right] \exp \left[ - \left( \frac{W^\infty}{\phi} \right)^m \right] \\ & + \gamma \Delta \mathbf{S}^{(0)}(t) - \sum_{n=1}^N \alpha_n \mathbf{H}^{(n)}(t - \Delta t) \end{aligned} \tag{23}$$

where  $\eta = 1 - \sum_{n=1}^N \delta_n$  and  $\gamma = \sum_{n=1}^N \beta_n \delta_n$ .

In this equation,

$$\Delta W^\infty = \eta \Delta W^{(0)} = \eta \frac{\partial W^{(0)}}{\partial \mathbf{C}} : \Delta \mathbf{C} = \frac{\eta}{2} \mathbf{S}^{(0)} : \Delta \mathbf{C} \tag{24}$$

By collecting all terms that are multiplying  $\Delta \mathbf{C}$  and employing (19), the following expression for  $\Delta \mathbf{S}$  at time  $t$  is obtained:

$$\begin{aligned} \Delta \mathbf{S}(t) = & \frac{1}{2} \left\{ \eta \left[ \mathbf{D}^{(0)} - \frac{\eta m}{\phi^m} (W^\infty)^{m-1} \mathbf{S}^{(0)} \otimes \mathbf{S}^{(0)} \right] \exp \left[ - \left( \frac{W^\infty}{\phi} \right)^m \right] + \gamma \mathbf{D}^{(0)} \right\} : \Delta \mathbf{C} \\ & - \sum_{n=1}^N \alpha_n \mathbf{H}^{(n)}(t - \Delta t) \end{aligned} \tag{25}$$

This equation can be represented in the compact form:

$$\Delta \mathbf{S}(t) = \frac{1}{2} \mathbf{D} : \Delta \mathbf{C} - \Delta \mathbf{Q}(t) \tag{26}$$

where

$$\mathbf{D} = \eta \left[ \mathbf{D}^{(0)} - \frac{\eta m}{\phi^m} (W^\infty)^{m-1} \mathbf{S}^{(0)} \otimes \mathbf{S}^{(0)} \right] \exp \left[ - \left( \frac{W^\infty}{\phi} \right)^m \right] + \gamma \mathbf{D}^{(0)}$$

$$\Delta \mathbf{Q}(t) = \sum_{n=1}^N \alpha_n \mathbf{H}^{(n)}(t - \Delta t) \quad (27)$$

It should be noted that the viscoelastic contribution  $\Delta \mathbf{Q}$  is indeed a small increment since  $\alpha_n \approx \Delta t / \tau_n$ .

The following special cases can be obtained:

1. Viscoelastic material without strain energy limiter ( $\phi \rightarrow \infty$ ). In this case, (26) is applicable with:

$$\mathbf{D} = \left[ 1 - \sum_{n=1}^N \delta_n (1 - \beta_n) \right] \mathbf{D}^{(0)} \quad (28)$$

2. Hyperelastic material whose strain energy is  $W$  with energy limiter ( $\delta_n = 0$ ). Here, the second Piola-Kirchhoff  $\mathbf{S}$  is given by:

$$\mathbf{S} = 2 \frac{\partial W}{\partial \mathbf{C}} \exp \left[ - \left( \frac{W}{\phi} \right)^m \right] \quad (29)$$

and Eq. 26 reduces to:

$$\Delta \mathbf{S} = \frac{1}{2} \mathbf{D} : \Delta \mathbf{C} \quad (30)$$

with

$$\mathbf{D} = \left[ 4 \frac{\partial^2 W}{\partial \mathbf{C} \partial \mathbf{C}} - \frac{m}{\phi^m} W^{m-1} \mathbf{S} \otimes \mathbf{S} \right] \exp \left[ - \left( \frac{W}{\phi} \right)^m \right] \quad (31)$$

which in the absence of a strain energy limiter reduces to  $\mathbf{D} = 4 \partial^2 W / \partial \mathbf{C} \partial \mathbf{C}$ .

The first Piola-Kirchhoff  $\mathbf{T}$  is given, [12], by:

$$\mathbf{T} = \mathbf{S} \mathbf{F}^T \quad (32)$$

Therefore, its increment can be established in the form:

$$\Delta \mathbf{T} = \mathbf{R} : \Delta \mathbf{F} - \Delta \mathbf{V} \quad (33)$$

where the components of the first tangent tensor  $\mathbf{R}$  are given by:

$$R_{ijkl} = D_{irls} F_{jr} F_{ks} + S_{il} \delta_{jk} \quad (34)$$

with  $\delta_{jk}$  being the Kronecker delta, and

$$\Delta \mathbf{V} = \Delta \mathbf{Q} \mathbf{F}^T \quad (35)$$

By defining the vectors:

$$\begin{aligned} \Delta \boldsymbol{\Omega} &= [\Delta F_{11}, \Delta F_{12}, \Delta F_{13}, \Delta F_{21}, \Delta F_{22}, \Delta F_{23}, \Delta F_{31}, \Delta F_{32}, \Delta F_{33}] \\ \Delta \boldsymbol{\Sigma} &= [\Delta T_{11}, \Delta T_{12}, \Delta T_{13}, \Delta T_{21}, \Delta T_{22}, \Delta T_{23}, \Delta T_{31}, \Delta T_{32}, \Delta T_{33}] \\ \Delta \mathbf{G} &= [\Delta V_{11}, \Delta V_{12}, \Delta V_{13}, \Delta V_{21}, \Delta V_{22}, \Delta V_{23}, \Delta V_{31}, \Delta V_{32}, \Delta V_{33}] \end{aligned} \quad (36)$$

constitutive (33) can be written in the matrix form:

$$\Delta \boldsymbol{\Sigma} = \mathbf{Z} \Delta \boldsymbol{\Omega} - \Delta \mathbf{G} \quad (37)$$

where  $\mathbf{Z}$  is the 9th-order instantaneous matrix of the viscoelastic material which can be constructed from the first tangent tensor  $\mathbf{R}$  in Eq. (33).

The governing equations consist of the equilibrium equations which in the absence of body forces are given by:

$$\nabla \cdot \mathbf{T} = 0, \quad \text{or} \quad \frac{\partial T_{ji}}{\partial X_j} = 0 \quad (38)$$

Finally, in the absence of mechanical boundary traction, the mechanical tractions  $\mathbf{P} \cdot \mathbf{N}$ , with  $\mathbf{N}$  being the unit normal to the surface in the initial configuration, and the components of the mechanical displacement  $\mathbf{u}$  should be continuous across an interface between two materials. These interfacial conditions can be expressed in terms of jumps as follows:

$$[[\mathbf{T}^T]] \cdot \mathbf{N} = \mathbf{0}, \quad [[\mathbf{u}]] = 0 \tag{39}$$

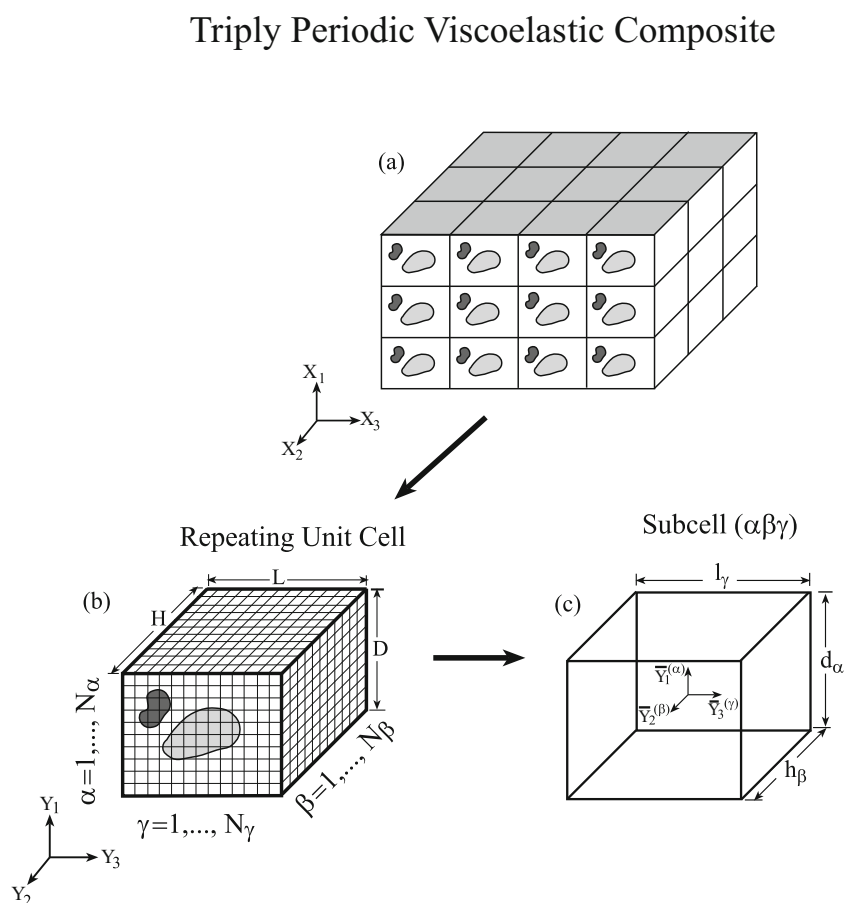
### 4 Finite strain micromechanical analysis of viscoelastic composites

Consider a multiphase composite in which the phases are viscoelastic materials undergoing large deformations. It is assumed that the composite microstructures are distributed periodically in the space and are described with respect to the global initial coordinates  $(X_1, X_2, X_3)$ ; see Fig. 1a. Figure 1b shows a repeating unit cell (RUC), defined with respect to local initial coordinates  $(Y_1, Y_2, Y_3)$ , of the periodic composite. Herein, the finite strain HFGMC micromechanical model is employed to predict the effective viscoelastic behavior of the composite caused by the application of external loading. The parallelepiped RUC of the composite is divided into  $N_\alpha, N_\beta,$  and  $N_\gamma$  subcells in the  $Y_1, Y_2,$  and  $Y_3$  directions, respectively. Each subcell is labeled by the indices  $(\alpha\beta\gamma)$  with  $\alpha = 1, \dots, N_\alpha, \beta = 1, \dots, N_\beta,$  and  $\gamma = 1, \dots, N_\gamma$ . The dimensions of subcell  $(\alpha\beta\gamma)$  in the  $Y_1, Y_2,$  and  $Y_3$  directions are denoted by  $d_\alpha, h_\beta,$  and  $l_\gamma$ , respectively. A local coordinate system  $(\bar{Y}_1^{(\alpha)}, \bar{Y}_2^{(\beta)}, \bar{Y}_3^{(\gamma)})$  is introduced in each subcell whose origin is located at its center; see Fig. 1c.

In the framework of HFGMC analysis which is presently employed to predict the effective behavior of the viscoelastic composite, the increments of the mechanical displacements  $\Delta \mathbf{u}^{(\alpha\beta\gamma)}$  in the subcell  $(\alpha\beta\gamma)$  are expanded into second-order polynomials. To this end, let the vector  $\Delta \mathbf{W}^{(\alpha\beta\gamma)}$  represent the components of the displacement vector  $\Delta \mathbf{u}^{(\alpha\beta\gamma)}$ :

$$\Delta \mathbf{W}^{(\alpha\beta\gamma)} = [\Delta u_1, \Delta u_2, \Delta u_3]^{(\alpha\beta\gamma)} \tag{40}$$

**Fig. 1** **a** A triply-periodic viscoelastic composite, defined with respect to global initial coordinates  $(X_1, X_2, X_3)$ . **b** A repeating unit cell (RUC), represented with respect to local initial coordinates  $(Y_1, Y_2, Y_3)$ . It is divided into  $N_\alpha, N_\beta,$  and  $N_\gamma$  subcells, in the  $Y_1, Y_2,$  and  $Y_3$  directions, respectively. **c** A characteristic subcell  $(\alpha\beta\gamma)$  with initial local coordinates  $\bar{Y}_1^{(\alpha)}, \bar{Y}_2^{(\beta)}$  and  $\bar{Y}_3^{(\gamma)}$  whose origin is located at its center



The 2nd-order expansion is given by:

$$\begin{aligned} \Delta \mathbf{W}^{(\alpha\beta\gamma)} &= \Delta \bar{\mathbf{W}} + \Delta \mathbf{W}_{(000)}^{(\alpha\beta\gamma)} + \bar{Y}_1^{(\alpha)} \Delta \mathbf{W}_{(100)}^{(\alpha\beta\gamma)} + \bar{Y}_2^{(\beta)} \Delta \mathbf{W}_{(010)}^{(\alpha\beta\gamma)} + \bar{Y}_3^{(\gamma)} \Delta \mathbf{W}_{(001)}^{(\alpha\beta\gamma)} \\ &+ \frac{1}{2} (3\bar{Y}_1^{(\alpha)2} - \frac{d_\alpha^2}{4}) \Delta \mathbf{W}_{(200)}^{(\alpha\beta\gamma)} + \frac{1}{2} (3\bar{Y}_2^{(\beta)2} - \frac{h_\beta^2}{4}) \Delta \mathbf{W}_{(020)}^{(\alpha\beta\gamma)} + \frac{1}{2} (3\bar{Y}_3^{(\gamma)2} - \frac{l_\gamma^2}{4}) \Delta \mathbf{W}_{(002)}^{(\alpha\beta\gamma)} \end{aligned} \tag{41}$$

where  $\Delta \bar{\mathbf{W}} = [\Delta \bar{\mathbf{F}} \cdot \mathbf{X}]$  consists of the externally applied loading, and the unknown coefficients  $\Delta \mathbf{W}_{(lmn)}^{(\alpha\beta\gamma)}$  are determined, as shown in the following, by implementing the equilibrium (38) together with the interfacial continuity conditions (39), and periodic conditions which are discussed as follows.

In the framework of the HFGMC micromechanical analysis, periodic boundary conditions must be imposed to ensure the periodic microstructure character of the composite which is represented by the repeating unit cell of Fig. 1b. These conditions require that the displacement vectors  $\mathbf{u}$  and the traction vectors  $\mathbf{T}^N = \mathbf{T}^T \cdot \mathbf{N}$  at the opposite edges of the repeating unit cell are identical. These imply that:

$$\begin{aligned} \mathbf{u}(Y_1 = 0) &= \mathbf{u}(Y_1 = D), & \mathbf{T}^N(Y_1 = 0) &= \mathbf{T}^N(Y_1 = D) \\ \mathbf{u}(Y_2 = 0) &= \mathbf{u}(Y_2 = H), & \mathbf{T}^N(Y_2 = 0) &= \mathbf{T}^N(Y_2 = H) \\ \mathbf{u}(Y_3 = 0) &= \mathbf{u}(Y_3 = L), & \mathbf{T}^N(Y_3 = 0) &= \mathbf{T}^N(Y_3 = L) \end{aligned} \tag{42}$$

The components of the deformation gradient tensor  $\mathbf{F}^{(\alpha\beta\gamma)}$  in the subcell  $(\alpha\beta\gamma)$  are determined from Eq. 41 by applying the relevant derivatives with respect to the local coordinates as follows:

$$\begin{aligned} \Delta F_{11}^{(\alpha\beta\gamma)} &= \Delta \bar{F}_{11} + \Delta W_{1(100)}^{(\alpha\beta\gamma)} + 3\bar{Y}_1^{(\alpha)} \Delta W_{1(200)}^{(\alpha\beta\gamma)} \\ \Delta F_{12}^{(\alpha\beta\gamma)} &= \Delta \bar{F}_{12} + \Delta W_{1(010)}^{(\alpha\beta\gamma)} + 3\bar{Y}_2^{(\gamma)} \Delta W_{1(020)}^{(\alpha\beta\gamma)} \\ \Delta F_{13}^{(\alpha\beta\gamma)} &= \Delta \bar{F}_{13} + \Delta W_{1(001)}^{(\alpha\beta\gamma)} + 3\bar{Y}_3^{(\gamma)} \Delta W_{1(002)}^{(\alpha\beta\gamma)} \\ \Delta F_{21}^{(\alpha\beta\gamma)} &= \Delta \bar{F}_{21} + \Delta W_{2(100)}^{(\alpha\beta\gamma)} + 3\bar{Y}_1^{(\alpha)} \Delta W_{2(200)}^{(\alpha\beta\gamma)} \\ \Delta F_{22}^{(\alpha\beta\gamma)} &= \Delta \bar{F}_{22} + \Delta W_{2(010)}^{(\alpha\beta\gamma)} + 3\bar{Y}_2^{(\gamma)} \Delta W_{2(020)}^{(\alpha\beta\gamma)} \\ \Delta F_{23}^{(\alpha\beta\gamma)} &= \Delta \bar{F}_{23} + \Delta W_{2(001)}^{(\alpha\beta\gamma)} + 3\bar{Y}_3^{(\gamma)} \Delta W_{2(002)}^{(\alpha\beta\gamma)} \\ \Delta F_{31}^{(\alpha\beta\gamma)} &= \Delta \bar{F}_{31} + \Delta W_{3(100)}^{(\alpha\beta\gamma)} + 3\bar{Y}_1^{(\alpha)} \Delta W_{3(200)}^{(\alpha\beta\gamma)} \\ \Delta F_{32}^{(\alpha\beta\gamma)} &= \Delta \bar{F}_{32} + \Delta W_{3(010)}^{(\alpha\beta\gamma)} + 3\bar{Y}_2^{(\gamma)} \Delta W_{3(020)}^{(\alpha\beta\gamma)} \\ \Delta F_{33}^{(\alpha\beta\gamma)} &= \Delta \bar{F}_{33} + \Delta W_{3(001)}^{(\alpha\beta\gamma)} + 3\bar{Y}_3^{(\gamma)} \Delta W_{3(002)}^{(\alpha\beta\gamma)} \end{aligned} \tag{43}$$

By averaging the increments of the equilibrium (38) over the volume of the subcell, the following relations are obtained:

$$\Delta \mathbf{I}_{1(000)}^{(\alpha\beta\gamma)} + \Delta \mathbf{I}_{2(000)}^{(\alpha\beta\gamma)} + \Delta \mathbf{I}_{3(000)}^{(\alpha\beta\gamma)} = 0 \tag{44}$$

where  $\Delta \mathbf{I}_{1(000)}^{(\alpha\beta\gamma)}$ ,  $\Delta \mathbf{I}_{2(000)}^{(\alpha\beta\gamma)}$ , and  $\Delta \mathbf{I}_{3(000)}^{(\alpha\beta\gamma)}$  can be expressed in terms of the surface-average of the traction increments evaluated along  $\bar{Y}_1^{(\alpha)} = \pm d_\alpha/2$ ,  $\bar{Y}_2^{(\beta)} = \pm h_\beta/2$ , and  $\bar{Y}_3^{(\gamma)} = \pm l_\gamma/2$ , respectively. Thus,

$$\begin{aligned} \Delta \mathbf{I}_{1(000)}^{(\alpha\beta\gamma)} &= \frac{1}{d_\alpha} \left[ \Delta \mathbf{T}_1^{+(\alpha\beta\gamma)} - \Delta \mathbf{T}_1^{-(\alpha\beta\gamma)} \right] \\ \Delta \mathbf{I}_{2(000)}^{(\alpha\beta\gamma)} &= \frac{1}{h_\beta} \left[ \Delta \mathbf{T}_2^{+(\alpha\beta\gamma)} - \Delta \mathbf{T}_2^{-(\alpha\beta\gamma)} \right] \\ \Delta \mathbf{I}_{3(000)}^{(\alpha\beta\gamma)} &= \frac{1}{l_\gamma} \left[ \Delta \mathbf{T}_3^{+(\alpha\beta\gamma)} - \Delta \mathbf{T}_3^{-(\alpha\beta\gamma)} \right] \end{aligned} \tag{45}$$



where the surface-average of the traction increments is given by:

$$\begin{aligned}
 \Delta \mathbf{T}_1^{\pm(\alpha\beta\gamma)} &= \frac{1}{h_\beta l_\gamma} \int_{-h_\beta/2}^{h_\beta/2} \int_{-l_\gamma/2}^{l_\gamma/2} \Delta \Sigma_1^{(\alpha\beta\gamma)} \left( \bar{Y}_1^{(\alpha)} = \pm \frac{d_\alpha}{2} \right) d\bar{Y}_2^{(\beta)} d\bar{Y}_3^{(\gamma)} \\
 \Delta \mathbf{T}_2^{\pm(\alpha\beta\gamma)} &= \frac{1}{d_\alpha l_\gamma} \int_{-d_\alpha/2}^{d_\alpha/2} \int_{-l_\gamma/2}^{l_\gamma/2} \Delta \Sigma_2^{(\alpha\beta\gamma)} \left( \bar{Y}_2^{(\beta)} = \pm \frac{h_\beta}{2} \right) d\bar{Y}_1^{(\alpha)} d\bar{Y}_3^{(\gamma)} \\
 \Delta \mathbf{T}_3^{\pm(\alpha\beta\gamma)} &= \frac{1}{d_\alpha h_\beta} \int_{-d_\alpha/2}^{d_\alpha/2} \int_{-h_\beta/2}^{h_\beta/2} \Delta \Sigma_3^{(\alpha\beta\gamma)} \left( \bar{Y}_3^{(\gamma)} = \pm \frac{l_\gamma}{2} \right) d\bar{Y}_1^{(\alpha)} d\bar{Y}_2^{(\beta)}
 \end{aligned} \tag{46}$$

and

$$\begin{aligned}
 \Delta \Sigma_1^{(\alpha\beta\gamma)} &= [\Delta T_{11}, \Delta T_{12}, \Delta T_{13}]^{(\alpha\beta\gamma)} \\
 \Delta \Sigma_2^{(\alpha\beta\gamma)} &= [\Delta T_{21}, \Delta T_{22}, \Delta T_{23}]^{(\alpha\beta\gamma)} \\
 \Delta \Sigma_3^{(\alpha\beta\gamma)} &= [\Delta T_{31}, \Delta T_{32}, \Delta T_{33}]^{(\alpha\beta\gamma)}
 \end{aligned} \tag{47}$$

The three vectors  $\Delta \Sigma_1^{(\alpha\beta\gamma)}$ ,  $\Delta \Sigma_2^{(\alpha\beta\gamma)}$ , and  $\Delta \Sigma_3^{(\alpha\beta\gamma)}$  include the traction increments acting on the surfaces whose normals are in the  $\bar{Y}_1^{(\alpha)}$ ,  $\bar{Y}_2^{(\beta)}$ , and  $\bar{Y}_3^{(\gamma)}$  directions, respectively.

Substitution of Eq. 45 in Eq. 44 yields:

$$\frac{1}{d_\alpha} [\Delta \mathbf{T}_1^{+(\alpha\beta\gamma)} - \Delta \mathbf{T}_1^{-(\alpha\beta\gamma)}] + \frac{1}{h_\beta} [\Delta \mathbf{T}_2^{+(\alpha\beta\gamma)} - \Delta \mathbf{T}_2^{-(\alpha\beta\gamma)}] + \frac{1}{l_\gamma} [\Delta \mathbf{T}_3^{+(\alpha\beta\gamma)} - \Delta \mathbf{T}_3^{-(\alpha\beta\gamma)}] = 0 \tag{48}$$

This equation expresses the increments of the equilibrium equations which are imposed in the average sense within subcell  $(\alpha\beta\gamma)$ .

By employing the constitutive relations (37), the following expressions for the surface-average of the traction increments are obtained from Eqs. 43 and 46:

$$\begin{aligned}
 \Delta T_{1i}^{\pm(\alpha\beta\gamma)} &= Z_{i1}^{(\alpha\beta\gamma)} \left( \Delta W_{1(100)} \pm \frac{3d_\alpha}{2} \Delta W_{1(200)} \right)^{(\alpha\beta\gamma)} + Z_{i2}^{(\alpha\beta\gamma)} \Delta W_{1(010)}^{(\alpha\beta\gamma)} + Z_{i3}^{(\alpha\beta\gamma)} \Delta W_{1(001)}^{(\alpha\beta\gamma)} \\
 &+ Z_{i4}^{(\alpha\beta\gamma)} \left( \Delta W_{2(100)} \pm \frac{3d_\alpha}{2} \Delta W_{2(200)} \right)^{(\alpha\beta\gamma)} + Z_{i5}^{(\alpha\beta\gamma)} \Delta W_{2(010)}^{(\alpha\beta\gamma)} + Z_{i6}^{(\alpha\beta\gamma)} \Delta W_{2(001)}^{(\alpha\beta\gamma)} \\
 &+ Z_{i7}^{(\alpha\beta\gamma)} \left( \Delta W_{3(100)} \pm \frac{3d_\alpha}{2} \Delta W_{3(200)} \right)^{(\alpha\beta\gamma)} + Z_{i8}^{(\alpha\beta\gamma)} \Delta W_{3(010)}^{(\alpha\beta\gamma)} + Z_{i9}^{(\alpha\beta\gamma)} \Delta W_{3(001)}^{(\alpha\beta\gamma)} \\
 &+ \sum_{p=1}^9 Z_{ip}^{(\alpha\beta\gamma)} \Delta \bar{\Omega}_p - \Delta G_i^{(\alpha\beta\gamma)}
 \end{aligned} \tag{49}$$

where  $i = 1, 2, 3$ .

$$\begin{aligned}
 \Delta T_{2i}^{\pm(\alpha\beta\gamma)} &= Z_{k1}^{(\alpha\beta\gamma)} \Delta W_{1(100)}^{(\alpha\beta\gamma)} + Z_{k2}^{(\alpha\beta\gamma)} \left( \Delta W_{1(010)} \pm \frac{3h_\beta}{2} \Delta W_{1(020)} \right)^{(\alpha\beta\gamma)} + Z_{k3}^{(\alpha\beta\gamma)} \Delta W_{1(001)}^{(\alpha\beta\gamma)} \\
 &+ Z_{k4}^{(\alpha\beta\gamma)} \Delta W_{2(100)}^{(\alpha\beta\gamma)} + Z_{k5}^{(\alpha\beta\gamma)} \left( \Delta W_{2(010)} \pm \frac{3h_\beta}{2} \Delta W_{2(020)} \right)^{(\alpha\beta\gamma)} + Z_{k6}^{(\alpha\beta\gamma)} \Delta W_{2(001)}^{(\alpha\beta\gamma)} \\
 &+ Z_{k7}^{(\alpha\beta\gamma)} \Delta W_{3(100)}^{(\alpha\beta\gamma)} + Z_{k8}^{(\alpha\beta\gamma)} \left( \Delta W_{3(010)} \pm \frac{3h_\beta}{2} \Delta W_{3(020)} \right)^{(\alpha\beta\gamma)} + Z_{k9}^{(\alpha\beta\gamma)} \Delta W_{3(001)}^{(\alpha\beta\gamma)} \\
 &+ \sum_{p=1}^9 Z_{kp}^{(\alpha\beta\gamma)} \Delta \bar{\Omega}_p - \Delta G_k^{(\alpha\beta\gamma)}
 \end{aligned} \tag{50}$$

where  $i = 1 \rightarrow k = 4, i = 2 \rightarrow k = 5, i = 3 \rightarrow k = 6$ .

$$\begin{aligned} \Delta T_{3i}^{\pm(\alpha\beta\gamma)} &= Z_{k1}^{(\alpha\beta\gamma)} \Delta W_{1(100)}^{(\alpha\beta\gamma)} + Z_{k2}^{(\alpha\beta\gamma)} \Delta W_{1(010)}^{(\alpha\beta\gamma)} + Z_{k3}^{(\alpha\beta\gamma)} \left( \Delta W_{1(001)} \pm \frac{3l_\gamma}{2} \Delta W_{1(002)} \right)^{(\alpha\beta\gamma)} \\ &+ Z_{k4}^{(\alpha\beta\gamma)} \Delta W_{2(100)}^{(\alpha\beta\gamma)} + Z_{k5}^{(\alpha\beta\gamma)} \Delta W_{2(010)}^{(\alpha\beta\gamma)} + Z_{k6}^{(\alpha\beta\gamma)} \left( \Delta W_{2(001)} \pm \frac{3l_\gamma}{2} \Delta W_{2(002)} \right)^{(\alpha\beta\gamma)} \\ &+ Z_{k7}^{(\alpha\beta\gamma)} \Delta W_{3(100)}^{(\alpha\beta\gamma)} + Z_{k8}^{(\alpha\beta\gamma)} \Delta W_{3(010)}^{(\alpha\beta\gamma)} + Z_{k9}^{(\alpha\beta\gamma)} \left( \Delta W_{3(001)} \pm \frac{3l_\gamma}{2} \Delta W_{3(002)} \right)^{(\alpha\beta\gamma)} \\ &+ \sum_{p=1}^9 Z_{kp}^{(\alpha\beta\gamma)} \Delta \bar{\Omega}_p - \Delta G_k^{(\alpha\beta\gamma)} \end{aligned} \tag{51}$$

where  $i = 1 \rightarrow k = 7, i = 2 \rightarrow k = 8, i = 3 \rightarrow k = 9$ . In these equations,  $\Delta \bar{\Omega}$  represents the applied far-field:

$$\Delta \bar{\Omega} = [\Delta \bar{F}_{11}, \Delta \bar{F}_{12}, \Delta \bar{F}_{13}, \Delta \bar{F}_{21}, \Delta \bar{F}_{22}, \Delta \bar{F}_{23}, \Delta \bar{F}_{31}, \Delta \bar{F}_{32}, \Delta \bar{F}_{33}] \tag{52}$$

Substitution of Eqs. 49–51 in Eq. 48 provides the three relations:

$$\begin{aligned} &\left[ Z_{11} \Delta W_{1(200)} + Z_{14} \Delta W_{2(200)} + Z_{17} \Delta W_{3(200)} \right. \\ &+ Z_{22} \Delta W_{1(020)} + Z_{25} \Delta W_{2(020)} + Z_{28} \Delta W_{3(020)} \\ &\left. + Z_{33} \Delta W_{1(002)} + Z_{36} \Delta W_{2(002)} + Z_{39} \Delta W_{3(002)} \right]^{(\alpha\beta\gamma)} = 0 \end{aligned} \tag{53}$$

$$\begin{aligned} &\left[ Z_{41} \Delta W_{1(200)} + Z_{44} \Delta W_{2(200)} + Z_{47} \Delta W_{3(200)} \right. \\ &+ Z_{52} \Delta W_{1(020)} + Z_{55} \Delta W_{2(020)} + Z_{58} \Delta W_{3(020)} \\ &\left. + Z_{63} \Delta W_{1(002)} + Z_{66} \Delta W_{2(002)} + Z_{69} \Delta W_{3(002)} \right]^{(\alpha\beta\gamma)} = 0 \end{aligned} \tag{54}$$

$$\begin{aligned} &\left[ Z_{71} \Delta W_{1(200)} + Z_{74} \Delta W_{2(200)} + Z_{77} \Delta W_{3(200)} \right. \\ &+ Z_{82} \Delta W_{1(020)} + Z_{85} \Delta W_{2(020)} + Z_{88} \Delta W_{3(020)} \\ &\left. + Z_{93} \Delta W_{1(002)} + Z_{96} \Delta W_{2(002)} + Z_{99} \Delta W_{3(002)} \right]^{(\alpha\beta\gamma)} = 0 \end{aligned} \tag{55}$$

These three relations express the increments of the average equilibrium (38) in the subcell, which are given in terms of the increments of the unknown coefficients  $\Delta \mathbf{W}_{(lmn)}^{(\alpha\beta\gamma)}$ .

Similar to the increments of the surface-average tractions which were defined in Eq. 46, the surface-average displacement increments can be defined by:

$$\begin{aligned} \Delta \mathbf{U}_1^{\pm(\alpha\beta\gamma)} &= \frac{1}{h_\beta l_\gamma} \int_{-h_\beta/2}^{h_\beta/2} \int_{-l_\gamma/2}^{l_\gamma/2} \Delta \mathbf{W}^{(\alpha\beta\gamma)} \left( \bar{Y}_1^{(\alpha)} = \pm \frac{d_\alpha}{2} \right) d\bar{Y}_2^{(\beta)} d\bar{Y}_3^{(\gamma)} \\ \Delta \mathbf{U}_2^{\pm(\alpha\beta\gamma)} &= \frac{1}{d_\alpha l_\gamma} \int_{-d_\alpha/2}^{d_\alpha/2} \int_{-l_\gamma/2}^{l_\gamma/2} \Delta \mathbf{W}^{(\alpha\beta\gamma)} \left( \bar{Y}_2^{(\beta)} = \pm \frac{h_\beta}{2} \right) d\bar{Y}_1^{(\alpha)} d\bar{Y}_3^{(\gamma)} \\ \Delta \mathbf{U}_3^{\pm(\alpha\beta\gamma)} &= \frac{1}{d_\alpha h_\beta} \int_{-d_\alpha/2}^{d_\alpha/2} \int_{-h_\beta/2}^{h_\beta/2} \Delta \mathbf{W}^{(\alpha\beta\gamma)} \left( \bar{Y}_3^{(\gamma)} = \pm \frac{l_\gamma}{2} \right) d\bar{Y}_1^{(\alpha)} d\bar{Y}_2^{(\beta)} \end{aligned} \tag{56}$$

In the following, these increments of the surface-average quantities  $\Delta \mathbf{U}_i^{\pm(\alpha\beta\gamma)}$ ,  $i = 1, 2, 3$ , will be related to the microvariable increments  $\mathbf{W}_{(lmn)}^{(\alpha\beta\gamma)}$ ;  $(lmn) = 0, 1, 2$ ; in the expansions (41). To this end, by substituting (41) in Eq. 56, the following relations are obtained:

$$\begin{aligned} \Delta \mathbf{U}_1^{\pm(\alpha\beta\gamma)} &= \Delta \mathbf{W}_{(000)}^{(\alpha\beta\gamma)} \pm \frac{d_\alpha}{2} \Delta \mathbf{W}_{(100)}^{(\alpha\beta\gamma)} + \frac{d_\alpha^2}{4} \Delta \mathbf{W}_{(200)}^{(\alpha\beta\gamma)} \\ \Delta \mathbf{U}_2^{\pm(\alpha\beta\gamma)} &= \Delta \mathbf{W}_{(000)}^{(\alpha\beta\gamma)} \pm \frac{h_\beta}{2} \Delta \mathbf{W}_{(010)}^{(\alpha\beta\gamma)} + \frac{h_\beta^2}{4} \Delta \mathbf{W}_{(020)}^{(\alpha\beta\gamma)} \\ \Delta \mathbf{U}_3^{\pm(\alpha\beta\gamma)} &= \Delta \mathbf{W}_{(000)}^{(\alpha\beta\gamma)} \pm \frac{l_\gamma}{2} \Delta \mathbf{W}_{(001)}^{(\alpha\beta\gamma)} + \frac{l_\gamma^2}{4} \Delta \mathbf{W}_{(002)}^{(\alpha\beta\gamma)} \end{aligned} \tag{57}$$

Manipulations of Eq. 57 by subtractions and additions yield:

$$\begin{aligned} \Delta \mathbf{W}_{(100)}^{(\alpha\beta\gamma)} &= \frac{1}{d_\alpha} [\Delta \mathbf{U}_1^+ - \Delta \mathbf{U}_1^-]^{(\alpha\beta\gamma)} \\ \Delta \mathbf{W}_{(010)}^{(\alpha\beta\gamma)} &= \frac{1}{h_\beta} [\Delta \mathbf{U}_2^+ - \Delta \mathbf{U}_2^-]^{(\alpha\beta\gamma)} \\ \Delta \mathbf{W}_{(001)}^{(\alpha\beta\gamma)} &= \frac{1}{l_\gamma} [\Delta \mathbf{U}_3^+ - \Delta \mathbf{U}_3^-]^{(\alpha\beta\gamma)} \end{aligned} \tag{58}$$

and

$$\begin{aligned} \Delta \mathbf{W}_{(200)}^{(\alpha\beta\gamma)} &= \frac{2}{d_\alpha^2} [\Delta \mathbf{U}_1^+ + \Delta \mathbf{U}_1^-]^{(\alpha\beta\gamma)} - \frac{4}{d_\alpha^2} \Delta \mathbf{W}_{(000)}^{(\alpha\beta\gamma)} \\ \Delta \mathbf{W}_{(020)}^{(\alpha\beta\gamma)} &= \frac{2}{h_\beta^2} [\Delta \mathbf{U}_2^+ + \Delta \mathbf{U}_2^-]^{(\alpha\beta\gamma)} - \frac{4}{h_\beta^2} \Delta \mathbf{W}_{(000)}^{(\alpha\beta\gamma)} \\ \Delta \mathbf{W}_{(002)}^{(\alpha\beta\gamma)} &= \frac{2}{l_\gamma^2} [\Delta \mathbf{U}_3^+ + \Delta \mathbf{U}_3^-]^{(\alpha\beta\gamma)} - \frac{4}{l_\gamma^2} \Delta \mathbf{W}_{(000)}^{(\alpha\beta\gamma)} \end{aligned} \tag{59}$$

It is now possible to express  $\Delta \mathbf{W}_{(000)}^{(\alpha\beta\gamma)}$  in terms of the surface-average displacement increments  $\Delta \mathbf{U}_i^{\pm(\alpha\beta\gamma)}$ ;  $i = 1, 2, 3$ . This is achieved by substituting (58)–(59) in (53)–(55). As a result, a system of three linear algebraic equations in the three unknowns  $\Delta \mathbf{W}_{(000)}^{(\alpha\beta\gamma)}$  is obtained. The solution of this system of equations expresses these microvariables in terms of  $\Delta \mathbf{U}_i^{\pm(\alpha\beta\gamma)}$ . Hence, this solution together with Eqs. 58–59 can be represented as follows:

$$\begin{pmatrix} \Delta \mathbf{W}_{(000)}^{(\alpha\beta\gamma)} \\ \Delta \mathbf{W}_{(100)}^{(\alpha\beta\gamma)} \\ \Delta \mathbf{W}_{(010)}^{(\alpha\beta\gamma)} \\ \Delta \mathbf{W}_{(001)}^{(\alpha\beta\gamma)} \\ \Delta \mathbf{W}_{(200)}^{(\alpha\beta\gamma)} \\ \Delta \mathbf{W}_{(020)}^{(\alpha\beta\gamma)} \\ \Delta \mathbf{W}_{(002)}^{(\alpha\beta\gamma)} \end{pmatrix} = \mathbf{M}^{(\alpha\beta\gamma)} \begin{pmatrix} \Delta \mathbf{U}_1^+ - \Delta \mathbf{U}_1^- \\ \Delta \mathbf{U}_2^+ - \Delta \mathbf{U}_2^- \\ \Delta \mathbf{U}_3^+ - \Delta \mathbf{U}_3^- \end{pmatrix} \tag{60}$$

where  $\mathbf{M}_i^{(\alpha\beta\gamma)}$  are coefficient matrices whose elements are lengthy and therefore are not given.

Consequently, with expressions (60), the following relations can be established from Eqs. 49–51:

$$\begin{pmatrix} \Delta \mathbf{T}_1^\pm \\ \Delta \mathbf{T}_2^\pm \\ \Delta \mathbf{T}_3^\pm \end{pmatrix}^{(\alpha\beta\gamma)} = \mathbf{K}^{(\alpha\beta\gamma)} \begin{pmatrix} \Delta \mathbf{U}_1^\pm \\ \Delta \mathbf{U}_2^\pm \\ \Delta \mathbf{U}_3^\pm \end{pmatrix}^{(\alpha\beta\gamma)} + \begin{pmatrix} \Delta \Phi_1^\pm \\ \Delta \Phi_2^\pm \\ \Delta \Phi_3^\pm \end{pmatrix}^{(\alpha\beta\gamma)} + \begin{pmatrix} \Delta \mathbf{V}_1^\pm \\ \Delta \mathbf{V}_2^\pm \\ \Delta \mathbf{V}_3^\pm \end{pmatrix}^{(\alpha\beta\gamma)} \tag{61}$$

where  $\mathbf{K}^{(\alpha\beta\gamma)}$  is a square matrix of the 18th order which consists of the instantaneous properties  $\mathbf{Z}^{(\alpha\beta\gamma)}$  of the material filling subcell  $(\alpha\beta\gamma)$  and its geometrical dimensions. In these equations, the vectors  $\Delta\Phi_i^{\pm(\alpha\beta\gamma)}$ ,  $i = 1, 2, 3$ , are the far-field contributions. They are defined by:

$$\begin{aligned} \Delta\Phi_1^{\pm(\alpha\beta\gamma)} &= \begin{bmatrix} \sum_{p=1}^9 Z_{1p}^{(\alpha\beta\gamma)} \Delta\bar{\Omega}_p, & \sum_{p=1}^9 Z_{2p}^{(\alpha\beta\gamma)} \Delta\bar{\Omega}_p, & \sum_{p=1}^9 Z_{3p}^{(\alpha\beta\gamma)} \Delta\bar{\Omega}_p \\ \sum_{p=1}^9 Z_{4p}^{(\alpha\beta\gamma)} \Delta\bar{\Omega}_p, & \sum_{p=1}^9 Z_{5p}^{(\alpha\beta\gamma)} \Delta\bar{\Omega}_p, & \sum_{p=1}^9 Z_{6p}^{(\alpha\beta\gamma)} \Delta\bar{\Omega}_p \\ \sum_{p=1}^9 Z_{7p}^{(\alpha\beta\gamma)} \Delta\bar{\Omega}_p, & \sum_{p=1}^9 Z_{8p}^{(\alpha\beta\gamma)} \Delta\bar{\Omega}_p, & \sum_{p=1}^9 Z_{9p}^{(\alpha\beta\gamma)} \Delta\bar{\Omega}_p \end{bmatrix} \\ \Delta\Phi_2^{\pm(\alpha\beta\gamma)} &= \begin{bmatrix} \sum_{p=1}^9 Z_{1p}^{(\alpha\beta\gamma)} \Delta\bar{\Omega}_p, & \sum_{p=1}^9 Z_{2p}^{(\alpha\beta\gamma)} \Delta\bar{\Omega}_p, & \sum_{p=1}^9 Z_{3p}^{(\alpha\beta\gamma)} \Delta\bar{\Omega}_p \\ \sum_{p=1}^9 Z_{4p}^{(\alpha\beta\gamma)} \Delta\bar{\Omega}_p, & \sum_{p=1}^9 Z_{5p}^{(\alpha\beta\gamma)} \Delta\bar{\Omega}_p, & \sum_{p=1}^9 Z_{6p}^{(\alpha\beta\gamma)} \Delta\bar{\Omega}_p \\ \sum_{p=1}^9 Z_{7p}^{(\alpha\beta\gamma)} \Delta\bar{\Omega}_p, & \sum_{p=1}^9 Z_{8p}^{(\alpha\beta\gamma)} \Delta\bar{\Omega}_p, & \sum_{p=1}^9 Z_{9p}^{(\alpha\beta\gamma)} \Delta\bar{\Omega}_p \end{bmatrix} \\ \Delta\Phi_3^{\pm(\alpha\beta\gamma)} &= \begin{bmatrix} \sum_{p=1}^9 Z_{1p}^{(\alpha\beta\gamma)} \Delta\bar{\Omega}_p, & \sum_{p=1}^9 Z_{2p}^{(\alpha\beta\gamma)} \Delta\bar{\Omega}_p, & \sum_{p=1}^9 Z_{3p}^{(\alpha\beta\gamma)} \Delta\bar{\Omega}_p \\ \sum_{p=1}^9 Z_{4p}^{(\alpha\beta\gamma)} \Delta\bar{\Omega}_p, & \sum_{p=1}^9 Z_{5p}^{(\alpha\beta\gamma)} \Delta\bar{\Omega}_p, & \sum_{p=1}^9 Z_{6p}^{(\alpha\beta\gamma)} \Delta\bar{\Omega}_p \\ \sum_{p=1}^9 Z_{7p}^{(\alpha\beta\gamma)} \Delta\bar{\Omega}_p, & \sum_{p=1}^9 Z_{8p}^{(\alpha\beta\gamma)} \Delta\bar{\Omega}_p, & \sum_{p=1}^9 Z_{9p}^{(\alpha\beta\gamma)} \Delta\bar{\Omega}_p \end{bmatrix} \end{aligned} \tag{62}$$

Finally, the viscoelastic contributions are represented by  $\Delta\mathbf{V}_i^{\pm}$ ,  $i = 1, 2, 3$ : which are given by

$$\begin{aligned} \Delta\mathbf{V}_1^{\pm(\alpha\beta\gamma)} &= [\Delta G_1, \Delta G_2, \Delta G_3]^{(\alpha\beta\gamma)} \\ \Delta\mathbf{V}_2^{\pm(\alpha\beta\gamma)} &= [\Delta G_4, \Delta G_5, \Delta G_6]^{(\alpha\beta\gamma)} \\ \Delta\mathbf{V}_3^{\pm(\alpha\beta\gamma)} &= [\Delta G_7, \Delta G_8, \Delta G_9]^{(\alpha\beta\gamma)} \end{aligned} \tag{63}$$

The continuity conditions of surface-average displacement and the surface-average traction increments between neighboring subcells require that:

$$\begin{aligned} [\Delta\mathbf{U}_1 \ \Delta\mathbf{T}_1]^{+(\alpha\beta\gamma)} &= [\Delta\mathbf{U}_1 \ \Delta\mathbf{T}_1]^{-(\alpha+1 \ \beta \ \gamma)}, \quad \alpha = 1, \dots, N_\alpha - 1, \beta = 1, \dots, N_\beta, \gamma = 1, \dots, N_\gamma \\ [\Delta\mathbf{U}_2 \ \Delta\mathbf{T}_2]^{+(\alpha\beta\gamma)} &= [\Delta\mathbf{U}_2 \ \Delta\mathbf{T}_2]^{-(\alpha \ \beta+1 \ \gamma)}, \quad \alpha = 1, \dots, N_\alpha, \beta = 1, \dots, N_\beta - 1, \gamma = 1, \dots, N_\gamma \\ [\Delta\mathbf{U}_3 \ \Delta\mathbf{T}_3]^{+(\alpha\beta\gamma)} &= [\Delta\mathbf{U}_3 \ \Delta\mathbf{T}_3]^{-(\alpha \ \beta \ \gamma+1)}, \quad \alpha = 1, \dots, N_\alpha, \beta = 1, \dots, N_\beta, \gamma = 1, \dots, N_\gamma - 1 \end{aligned} \tag{64}$$

Next, the periodicity conditions that require the equality of the surface-average displacement increments as well as the surface-average traction increments at the opposite sides of the RUC are:

$$\begin{aligned} [\Delta\mathbf{U}_1 \ \Delta\mathbf{T}_1]^{-(1\beta\gamma)} &= [\Delta\mathbf{U}_1 \ \Delta\mathbf{T}_1]^{+(N_\alpha \ \beta \ \gamma)}, \quad \beta = 1, \dots, N_\beta, \gamma = 1, \dots, N_\gamma \\ [\Delta\mathbf{U}_2 \ \Delta\mathbf{T}_2]^{-(\alpha 1\gamma)} &= [\Delta\mathbf{U}_2 \ \Delta\mathbf{T}_2]^{+(\alpha \ N_\beta \ \gamma)}, \quad \alpha = 1, \dots, N_\alpha, \gamma = 1, \dots, N_\gamma \\ [\Delta\mathbf{U}_3 \ \Delta\mathbf{T}_3]^{-(\alpha\beta 1)} &= [\Delta\mathbf{U}_3 \ \Delta\mathbf{T}_3]^{+(\alpha \ \beta \ N_\gamma)}, \quad \alpha = 1, \dots, N_\alpha, \beta = 1, \dots, N_\beta \end{aligned} \tag{65}$$

Equations 64 and 65 form a system of  $18N_\alpha N_\beta N_\gamma$  algebraic equations in the same number of the surface-average displacement increments  $\Delta\mathbf{U}_1^{\pm(\alpha\beta\gamma)}$ ,  $\Delta\mathbf{U}_2^{\pm(\alpha\beta\gamma)}$  and  $\Delta\mathbf{U}_3^{\pm(\alpha\beta\gamma)}$  in all the subcells of the RUC (namely the composite). The solution at a current loading increment establishes the elastic instantaneous concentration tensors  $\mathbf{A}^{(\alpha\beta\gamma)}$  which relate the deformation gradient increments  $\Delta\boldsymbol{\Omega}^{(\alpha\beta\gamma)}$  in the subcell to the current externally applied far-field  $\Delta\bar{\boldsymbol{\Omega}}$  loading increments in the form:

$$\Delta\boldsymbol{\Omega}^{(\alpha\beta\gamma)} = \mathbf{A}^{(\alpha\beta\gamma)} : \Delta\bar{\boldsymbol{\Omega}} + \Delta\mathbf{A}^{V(\alpha\beta\gamma)} \tag{66}$$

where  $\Delta\mathbf{A}^{V(\alpha\beta\gamma)}$  are the increments of the viscoelastic contributions which can be determined at every time step when no mechanical loading is applied (i.e.,  $\Delta\bar{\boldsymbol{\Omega}} = \mathbf{0}$ ).

The average stress increments in the composite are given by:

$$\Delta\bar{\boldsymbol{\Sigma}} = \frac{1}{DHL} \sum_{\alpha=1}^{N_\alpha} \sum_{\beta=1}^{N_\beta} \sum_{\gamma=1}^{N_\gamma} d_\alpha h_\beta l_\gamma \Delta\boldsymbol{\Sigma}^{(\alpha\beta\gamma)} \tag{67}$$

Substituting the incremental constitutive (37) for  $\Delta\boldsymbol{\Sigma}^{(\alpha\beta\gamma)}$  in Eq. 67 and employing (66) yield:

$$\Delta\boldsymbol{\Sigma}^{(\alpha\beta\gamma)} = \mathbf{Z}^{(\alpha\beta\gamma)} : \left[ \mathbf{A}^{(\alpha\beta\gamma)} : \Delta\bar{\boldsymbol{\Omega}} + \Delta\mathbf{A}^{V(\alpha\beta\gamma)} \right] - \Delta\mathbf{G}^{(\alpha\beta\gamma)} \tag{68}$$

This establishes in the macroscopic (global) incremental constitutive equation of the viscoelastic composite:

$$\Delta\bar{\boldsymbol{\Sigma}} = \mathbf{Z}^* : \Delta\bar{\boldsymbol{\Omega}} - \Delta\bar{\mathbf{V}} \tag{69}$$

where  $\mathbf{Z}^*$  is the effective instantaneous tangent matrix of the composite which is given by:

$$\mathbf{Z}^* = \frac{1}{DHL} \sum_{\alpha=1}^{N_\alpha} \sum_{\beta=1}^{N_\beta} \sum_{\gamma=1}^{N_\gamma} d_\alpha h_\beta l_\gamma \mathbf{Z}^{(\alpha\beta\gamma)} : \mathbf{A}^{(\alpha\beta\gamma)} \tag{70}$$

The global increment of the viscoelastic contribution is expressed by:

$$\Delta \bar{\mathbf{V}} = -\frac{1}{DHL} \sum_{\alpha=1}^{N_\alpha} \sum_{\beta=1}^{N_\beta} \sum_{\gamma=1}^{N_\gamma} d_\alpha h_\beta l_\gamma \left[ \mathbf{Z}^{(\alpha\beta\gamma)} : \Delta \mathbf{A}^{V(\alpha\beta\gamma)} - \Delta \mathbf{G}^{(\alpha\beta\gamma)} \right] \tag{71}$$

The accuracy and reliability of the elastic finite strain HFGMC in the absence of energy limiter were verified in [2] in the presence of the Mullin effect and in [6] when the energy limiter was included. In these references, extensive comparisons of the predicted effective behaviors with analytical and numerical solutions were presented.

### 5 Applications

The proposed micromechanical analysis is presently applied for the prediction of the response of a viscoelastic composite that is subjected to various types of loading and rates. In the first class of applications, the composite is assumed to consist of a soft viscoelastic matrix reinforced by unidirectional elastic fibers. This is followed by predicting the response of a viscoelastic porous material. Finally, the creep behavior of the unidirectional composite under transverse and biaxial constant stress is investigated.

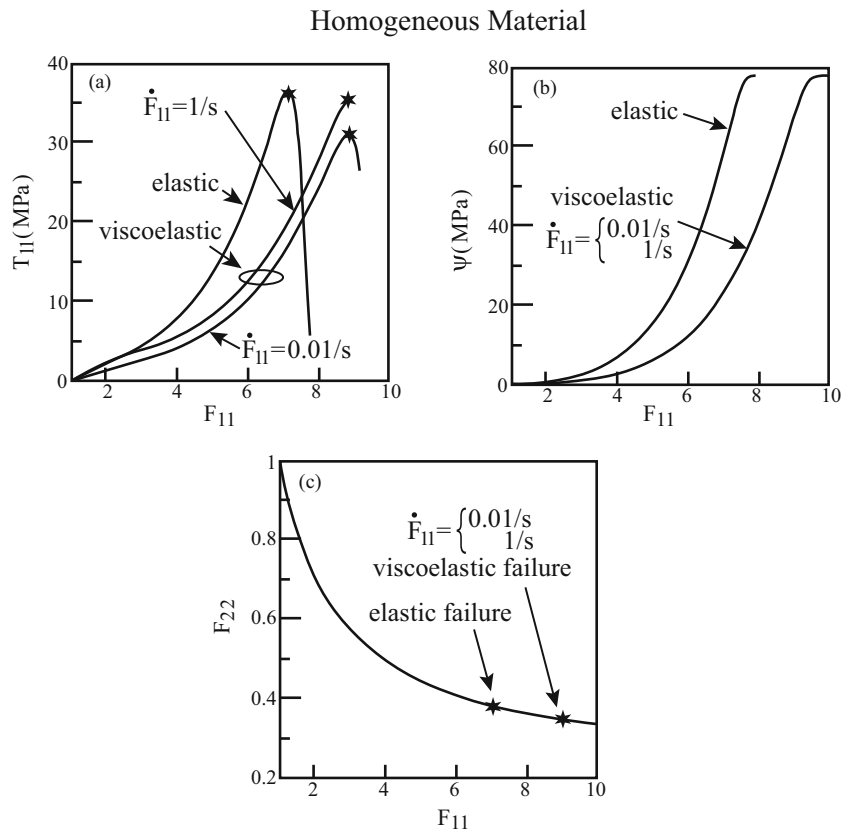
In all cases, the viscoelastic material is modeled by the short-term hyperelastic compressible [22] strain energy function  $W^{(0)}$ , Eq. 5, which for filled natural rubber has been characterized by [9]. It is given by:

$$W^{(0)} = \sum_{k=1}^3 C_k (\bar{I}_1 - 3)^k + \kappa (J - 1)^2 \tag{72}$$

where  $\bar{I}_1 = I_1/J^{2/3}$ ,  $I_1 = tr(\mathbf{C})$  being the first invariant of the right Cauchy-Green deformation tensor  $\mathbf{C}$ ,  $J = det(\mathbf{F})$  and  $\kappa$  represents the bulk modulus such that nearly incompressible material is obtained for large values of this constant. These material parameters are as follows:  $C_1 = 0.298$  MPa,  $C_2 = 0.014$  MPa, and  $C_3 = 0.00016$  MPa. The value of  $\kappa = 1$  GPa has been chosen which turns out to yield a determinant of deformation gradient which is very close to unity during the deformation process of the monolithic (unreinforced) rubber-like matrix. In addition, [9] observed that failure of the material in simple tension occurs when the value of the stretch in uniaxial tension is 7.12. The resulting response was therefore calibrated by [17] to determine the values of  $\phi$  and  $m$  in Eqs. 11 and 12. The recommended values  $\phi = 82$  MPa and  $m = 10$  have been chosen in the present article. This value of  $\phi$  has been obtained by a fit with the uniaxial tension test of [9]. The corresponding critical strain energy is  $\psi^c = 63.1$  MPa, and the energy of separation which is given by Eq. 11 is  $\psi^F = 78$  MPa. As to the viscoelastic effect, it is presently illustrated by choosing just one term  $N = 1$  in Eq. 6 with  $\delta_1 = 0.6$ . This choice implies that the equilibrium strain energy  $W^{(\infty)}$  is 0.4 of the initial short-time one  $W^{(0)}$ . In addition, a relaxation time  $\tau_1 = 0.25s$  is assumed in all applications.

In Fig. 2a, the stress-deformation gradient response of the viscoelastic material is shown for a uniaxial stress loading that is applied in the 1-direction at rates of  $\dot{F}_{11} = 0.01/s$  and  $\dot{F}_{11} = 1/s$ . Also shown in this figure is the corresponding elastic response of the material when the viscoelastic effects are neglected ( $\delta_1 = 0$ ). As shown, the stress rises gradually until it reaches a maximum value which corresponds to the failure stress of the material. The existence of the strain energy limiter causes a reduction of the stress at additional loading. The effect of the viscoelasticity is exhibited by the delayed approach of the material to failure which also depends upon the rate of loading. It is obvious that higher rates decrease the viscoelastic (viscous) effects. Figure 2b shows the enhanced strain energy functions  $\psi$ , Eq. 10, which rise with increasing loading, approaching their saturation values at the material failure. Finally, Fig. 2c exhibits the variations of the induced deformation gradient  $F_{22}$  (or  $F_{33}$ ) in the transverse direction with the applied loading in the axial direction  $F_{11}$ . The figure shows that the variations in the elastic and viscoelastic in both rates coincide, and the corresponding failure points in both cases are indicated. Finally, the resulting volumetric deformation  $F_{11} + F_{22} + F_{33}$  variation (not shown) caused by the application of the uniaxial stress loading at a rate of  $\dot{F}_{11} = 0.01/s$  rises almost linearly from 3 to about 9.9. Similar behavior is exhibited by the application of the uniaxial stress loading at a rate of  $\dot{F}_{11} = 1/s$ .

**Fig. 2** **a** The stress-deformation gradient response of the monolithic viscoelastic material to uniaxial stress loading, applied at two rates:  $\dot{F}_{11} = 0.01/s$  and  $\dot{F}_{11} = 1/s$ . Also shown is the response of the corresponding elastic material ( $\delta_1 = 0$ ). **b** The variations of the enhanced strain-energy functions in the viscoelastic and elastic cases. **c** The variation of the induced deformation gradient in the transverse direction  $F_{22}$  with applied deformation gradient in the axial direction  $F_{11}$ . The viscoelastic and elastic failure points are indicated



It should be noted that the incremental procedure of integrating (69) for the computation of the viscoelastic response is successful in providing the material behavior until failure occurrence. The response after reaching this point starts to descend rapidly followed by divergence of the procedure (caused by the negative tangent). In some cases (especially when analyzing composites), this divergence occurs immediately after reaching failure.

### 5.1 Viscoelastic response of unidirectional composite

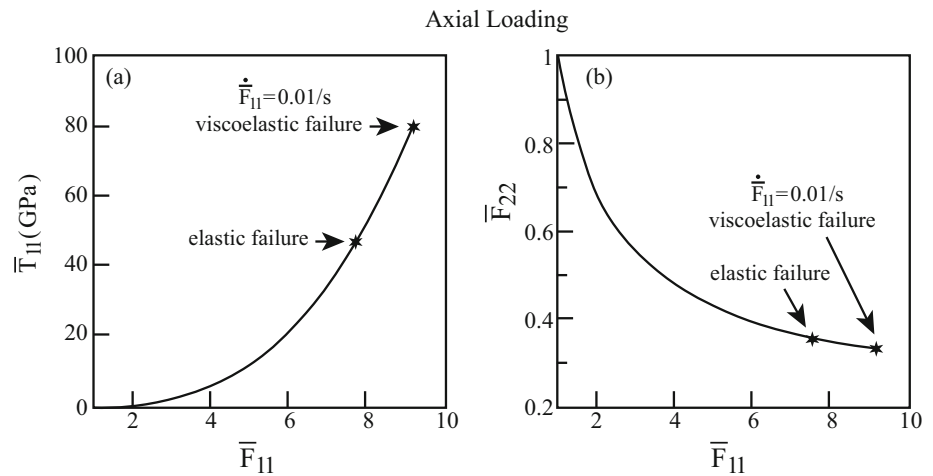
The reinforcing fibers in the unidirectional composite are assumed to be represented by a hyperelastic material whose strain energy function is given by St. Venant-Kirchhoff:

$$W = \frac{\lambda + 2\mu}{2} K_1^2 - 2\mu K_2 \tag{73}$$

where  $K_1 = (I_1 - 1)/2$  and  $K_2 = (-2I_1 + I_2 + 3)/4$ . By choosing  $\lambda = 2.85$  GPa and  $\mu = 0.71$  GPa, nylon fibers whose Young's modulus 2 GPa and Poisson's ratio 0.4 are obtained in the linear region. The high contrast between the properties of the fibers and the soft matrix should be noticed. The volume fraction of the fibers is chosen as  $v_f = 0.05$  which is characteristic for reinforced rubber.

Consider a unidirectional composite in which the fibers, modeled by Eq. 73, are oriented in the 1-direction. The soft matrix is the viscoelastic material which was previously described. For a uniaxial loading of the composite, the average (global) deformation gradient  $\bar{F}_{11}$  is applied at a rate of  $\dot{\bar{F}}_{11} = 0.01/s$  in the fiber direction while keeping all other directions tractions-free. The resulting global stress-deformation gradient response  $\bar{T}_{11} - \bar{F}_{11}$  is shown in Fig. 3a. Also shown in this figure is the corresponding elastic behavior ( $\delta_1 = 0$ ). The indicated failure of the composite in both cases shows that failure occurs in the viscoelastic composite at a later stage of loading. The resulting induced global deformations  $\bar{F}_{22}$  in the transverse direction to the fibers are shown in Fig. 3b in both cases together with the corresponding failure points. The reinforcement effect is clearly noticed by the ability of the composite to sustain high stresses. It is interesting to note that here too the viscoelastic effect enhances the composite ability to sustain loading and delays its failure. Since the behavior of unidirectional composites in the fiber direction is dominated by the fibers which are modeled by Eq. 73, it can be presently

**Fig. 3** **a** The global stress-deformation gradient response of the viscoelastic and elastic unidirectional composites to uniaxial stress loading in the fiber direction, applied at a rate of  $\dot{\bar{F}}_{11} = 0.01/s$ . **b** The variation of the induced global deformation gradient in the transverse direction  $\bar{F}_{22}$  to the fibers with the applied global deformation gradient in the axial direction  $\bar{F}_{11}$



concluded that the nonlinearity exhibited in Fig. 3a can be attributed to the response of the elastic fibers. It should be finally noted that whereas Fig. 3 presents the response of the composite when it is loaded at a rate of 0.01/s, but due to the elastic fibers dominance loading at a fast rate of 1/s did not modify this response.

For a uniaxial transverse loading in which  $\bar{F}_{22}$  is applied in the transverse 2-direction to the fibers at a rate of  $\dot{\bar{F}}_{22} = 0.01/s$  (while keeping all other directions tractions-free), the resulting response of the composite is shown in Fig. 4. Figure 4a compares the response and values of failure of the unidirectional viscoelastic composite with those of the elastic composite ( $\delta_1 = 0$ ). Compared with the elastic composite, here too this figure shows that the failure of the composite occurs at higher deformation and lower stress. Compared with the previously discussed uniaxial loading case of the viscoelastic composite in the fiber direction (failure at 80 GPa), the ability of the composite to sustain loading in the transverse direction is considerably lower (about 18 MPa). It is even lower than that of the unreinforced viscoelastic matrix (about 35 MPa). It should finally be noted (but not shown) the increase of the rate of loading in the transverse direction to  $\dot{\bar{F}}_{22} = 1/s$  decreases the failure stress to  $\bar{T}_{22} = 8.1$  MPa which is obtained at a deformation gradient of  $\bar{F}_{22} = 4$ .

Consider next a biaxial loading of the unidirectional composite which simultaneously loaded in the fiber direction and in the transverse direction such that  $\bar{F}_{11} = \bar{F}_{22}$  are prescribed, while keeping all the other stresses equal to zero. Figure 5 exhibits the composite response to this type of loading which is applied at a rate of  $\dot{\bar{F}}_{11} = \dot{\bar{F}}_{22} = 1/s$ . For the elastic

Transverse Loading

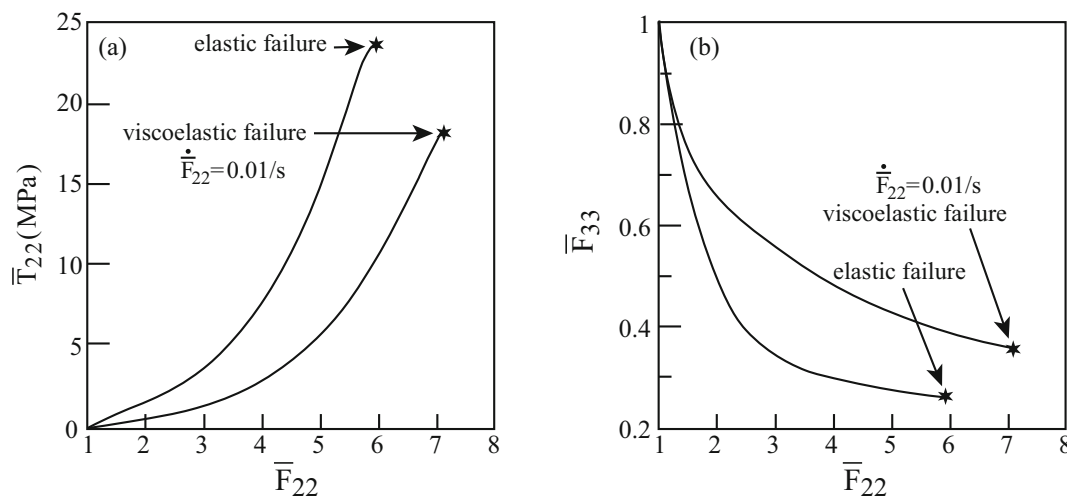


**Fig. 4** **a** The global stress-deformation gradient response of the viscoelastic and elastic unidirectional composite to uniaxial stress loading in the transverse direction to the fibers, applied at a rate of  $\dot{\bar{F}}_{22} = 0.01/s$ . **b** The variation of the induced global deformation gradient in the transverse direction  $\bar{F}_{33}$  with applied global deformation gradient in the transverse direction  $\bar{F}_{22}$

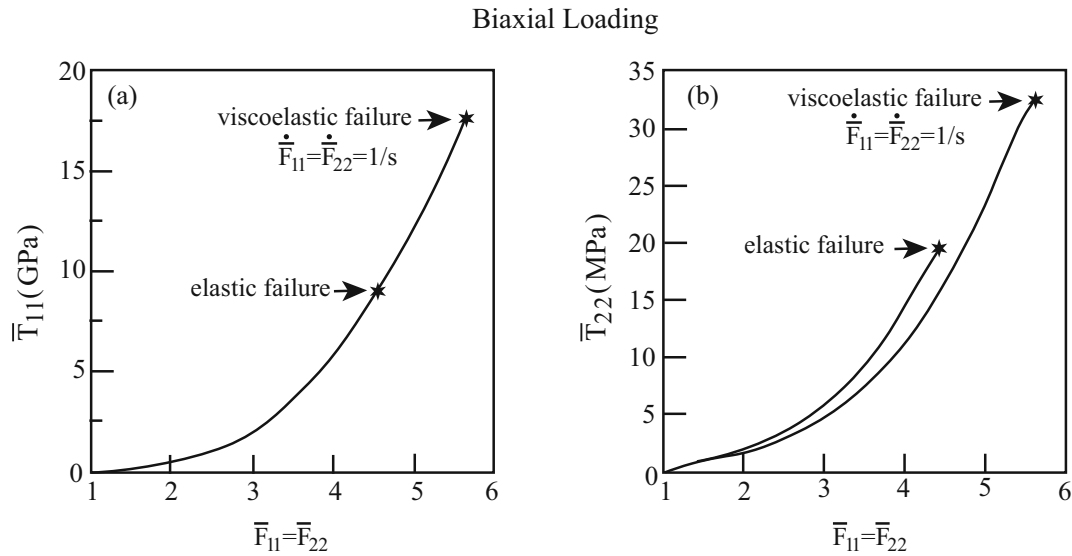
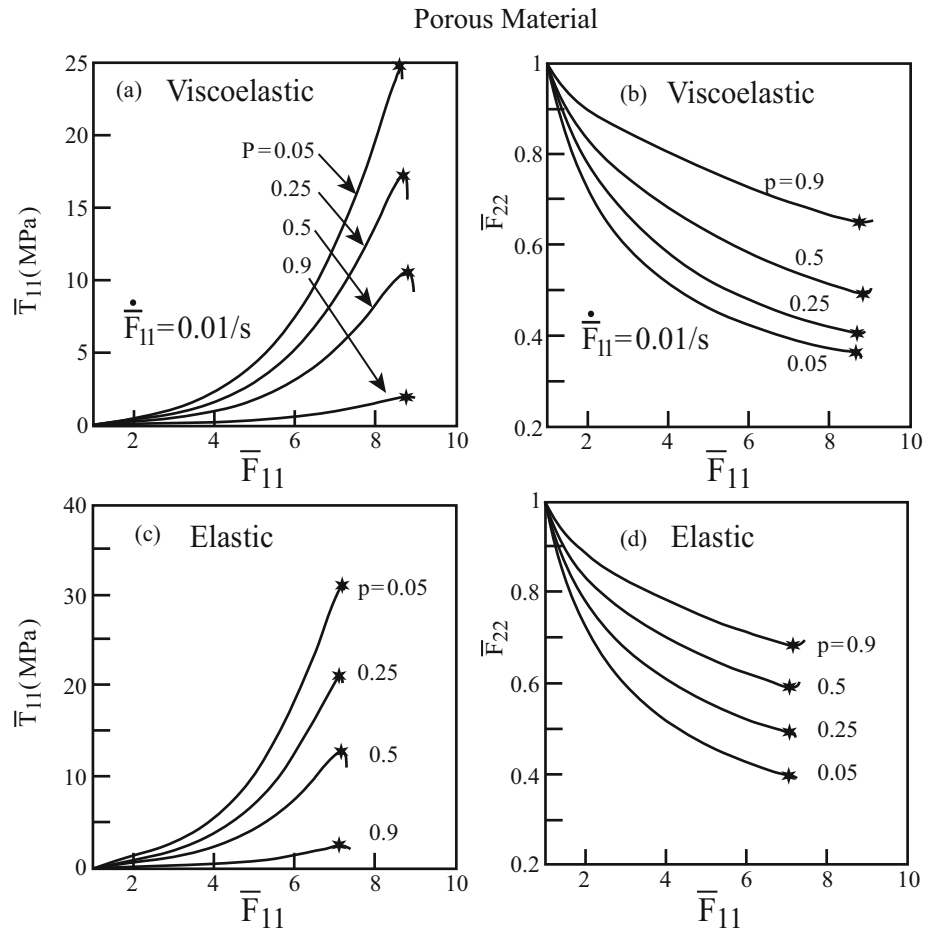


**Fig. 5** The global stress-deformation gradient response of the viscoelastic and elastic unidirectional composite to biaxial stress loading in the axial and transverse directions, applied at a rate of  $\dot{\bar{F}}_{11} = \dot{\bar{F}}_{22} = 1/s$ . **a**  $\bar{T}_{11}$  against  $\bar{F}_{11} = \bar{F}_{22}$ . **b**  $\bar{T}_{22}$  against  $\bar{F}_{11} = \bar{F}_{22}$

composite failure presently occurs at  $\bar{T}_{11} = 8.2$  GPa compared with  $\bar{T}_{11} = 40$  GPa, c.f., Fig. 3a, in the axial loading case. For the viscoelastic composite, on the other hand, failure presently takes place at  $\bar{T}_{11} = 18.1$  GPa compared with 80 GPa

**Fig. 6 a** The global stress-deformation gradient response of the viscoelastic porous material to uniaxial stress loading in the 1-direction, applied at a rate of  $\dot{\bar{F}}_{11} = 0.01/s$ , for various values of porosities. **b** The variation of the induced global deformation gradient in the transverse direction  $\bar{F}_{22}$  with applied global deformation gradient in the axial direction  $\bar{F}_{11}$  of the viscoelastic porous material. **c** The global stress-deformation gradient response of the elastic porous material to uniaxial stress loading in the 1-direction for various values of porosities. **d** The variation of the induced global deformation gradient in the transverse direction  $\bar{F}_{22}$  with applied global deformation gradient in the axial direction  $\bar{F}_{11}$  of the elastic porous material. The viscoelastic and elastic failure points are indicated





in the axial loading case. Thus, a considerable weakening of the composite is obtained in the fiber direction under biaxial loading. For the resulting transverse stress  $\bar{T}_{22}$  however, failure occurs at about 32 MPa. This is an improvement over the pure transverse loading for which, as mentioned above, failure at this value of loading rate takes place at  $\bar{T}_{22} = 8.1$  MPa at a deformation of  $\bar{F}_{22} = 4$ .

### 5.2 Viscoelastic response of porous materials

Porous viscoelastic materials can be modeled by the present analysis by selecting the central subcells in the repeating unit cell of Fig. 1b to possess vanishingly small stiffnesses. As a result, the previously discussed finite strain viscoelastic material whose short-term hyperelastic compressible strain energy function  $W^{(0)}$  is given by Eq. 72 with pores is obtained. In addition, the replacement of the strain energy by the enhanced function  $\psi$ , Eq. 10, limits the ability of the porous viscoelastic material to accumulate deformations which provides a mean to predict its failure.

Let the porous viscoelastic material be loaded in the 1-direction at a rate of  $\dot{\bar{F}}_{11} = 0.01/s$ . Figure 6a presents the global stress-deformation gradient  $\bar{T}_{11} - \bar{F}_{11}$  of the porous material for various amounts of porosities  $0.05 \leq p \leq 0.9$ . In each case, the failure stress is indicated. Corresponding to Fig. 6a and b exhibits the variations of induced transverse deformation gradient in the 2-direction for the same values of porosities. It should be interesting to compare the behavior of the viscoelastic porous material with that of the elastic porous one ( $\delta_1 = 0$ ). Figure 6c and d show the corresponding behavior of the elastic porous material together with the predicted values of failure stresses for each value of porosity. The comparison reveals that compared with the elastic case, failure of the viscoelastic porous material occurs at lower stresses and higher values of the applied deformation gradient.

**Fig. 7** a, b Creep behavior and the enhanced energy function  $\psi$  of the homogeneous viscoelastic material which is subjected to constant stress of  $T_{11} = 80$  MPa; c, d creep behavior and the enhanced energy function  $\psi$  of the viscoelastic unidirectional composite which is subjected to a constant transverse stress of  $\bar{T}_{22} = 40$  MPa. Also shown is the creep corresponding behavior of the homogeneous viscoelastic material under the same constant stress

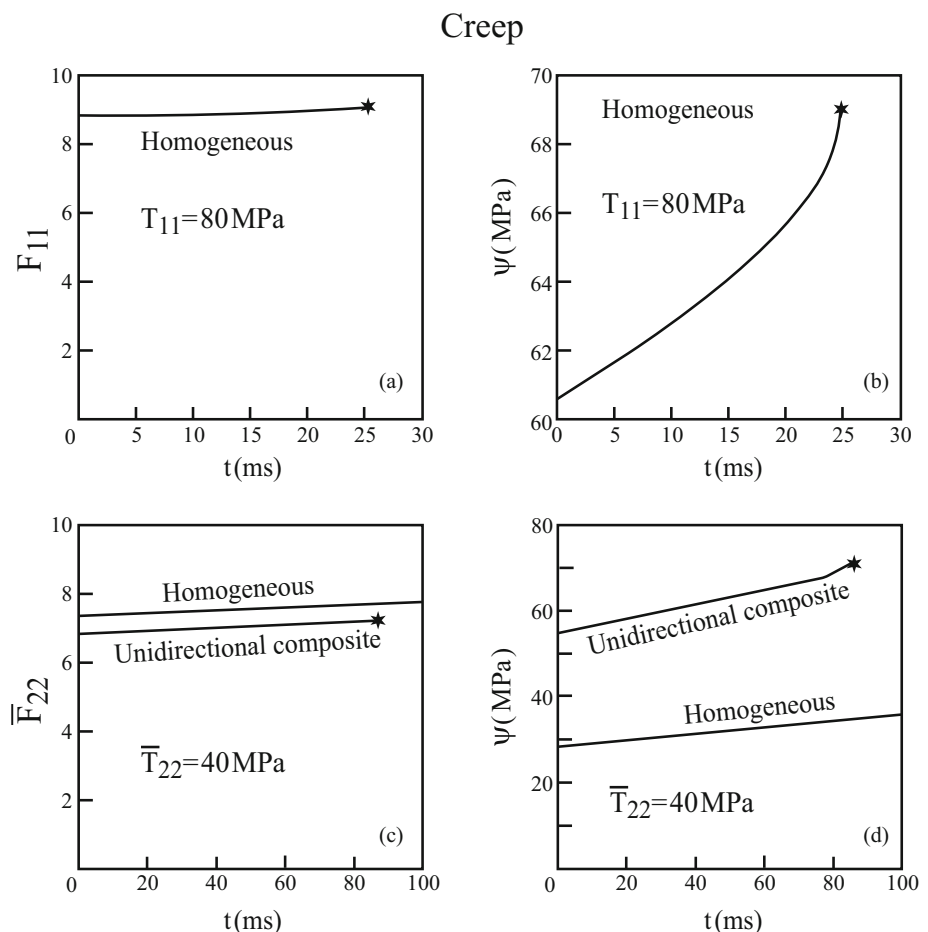
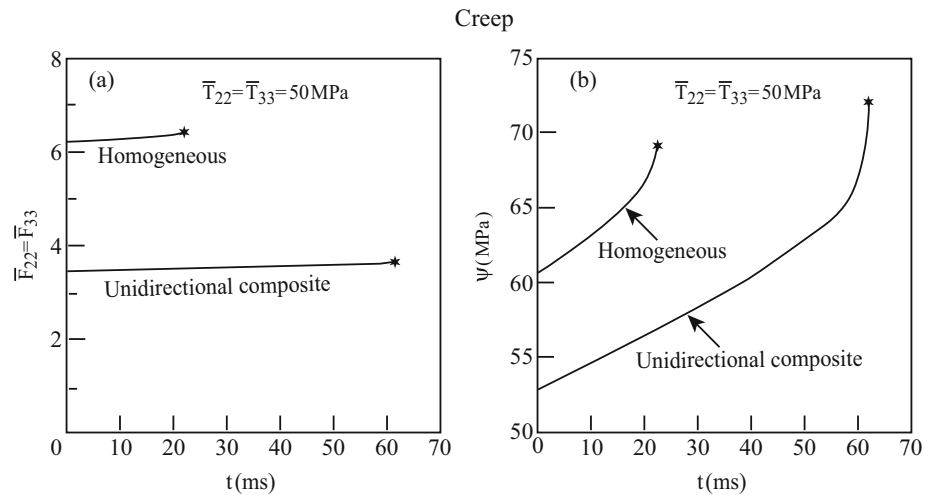


**Fig. 8 a, b** Creep behavior and the enhanced energy function  $\psi$  of the viscoelastic unidirectional composite which is subjected to a constant biaxial stresses of  $\bar{T}_{22} = \bar{T}_{33} = 50$  MPa. Also shown is the creep corresponding behavior of the homogeneous viscoelastic material under the same constant stress



### 5.3 Creep of viscoelastic unidirectional composite

Consider the viscoelastic unidirectional composite whose behavior was investigated and discussed in Section 5.1. The creep behavior of this composite and its homogeneous viscoelastic matrix can be investigated by applying a constant stress loading at given direction (e.g., at the transverse direction to the fibers) while keeping all other stress components equal to zero. The resulting deformation gradient against time exhibits the creep behavior of the composite. In addition, the time locations of failure can be predicted by the present micromechanical analysis, in conjunction with the enhanced strain energy function of the viscoelastic matrix.

Figure 7a shows the creep behavior of the homogeneous viscoelastic material that is subjected to a constant stress of  $T_{11} = 80$  MPa. As indicated, failure of the material takes place at time  $t = 26$  ms. Corresponding to this figure, it is interesting to observe the increase of the enhanced strain energy function  $\psi$ , Eq. 10, with time up to failure. This is shown in Fig. 7b in which the time to failure is rapidly approached.

The creep behavior of the viscoelastic unidirectional composite is shown in Fig. 7c for a constant stress of  $\bar{T}_{22} = 40$  MPa which is applied in the transverse direction to the fibers. Also shown in this figure is the corresponding creep of the homogeneous viscoelastic material under the same value of constant stress. It is readily observed that the composite fails at about  $t = 85$  ms whereas the homogeneous material does not fail but continue creeping. The variations of the associate strain energy functions in both cases are shown in Fig. 7d which clearly indicate whether failure is taking place or not.

As a final illustration, the creep behavior of the considered viscoelastic unidirectional composite is shown in Fig. 8a when it is subjected to biaxial transverse constant stresses of  $\bar{T}_{22} = \bar{T}_{33} = 50$  MPa. Also shown is the creep behavior of the homogeneous viscoelastic material under the same biaxial stresses. Compared with the homogeneous case, this figures shows that failure of the unidirectional composite takes place at a later time but at lower deformation gradients. The variations of the enhanced strain energy functions  $\psi$  of the viscoelastic unidirectional composite and the homogeneous material are shown in Fig. 8b. Approaching the failure times and their occurrence in both cases is well exhibited.

## 6 Conclusions

The constitutive relations that govern the global (macroscopic) response of viscoelastic multiphase composites undergoing large deformations have been established by employing the HFGMC micromechanical analysis. The energy function of the soft viscoelastic constituent of the composite is enhanced by a strain energy limiter which enforces its saturation. The occurrence of the saturation corresponds to the failure energy of the considered viscoelastic constituent. Thus, in conjunction with the micromechanical analysis, it is possible to predict the failure of the composite that is subjected to a given rate of an applied loading.

In the present investigation, perfect bonding between the constituents has been assumed. In practice, debonding can occur and its modeling can be implemented in the present micromechanical analysis in the same way as was performed in the analysis of elastic composites that was presented by [6].

The presently chosen finite strain viscoelastic model belongs to class which is referred to as finite linear viscoelasticity, c.f. [10], in which the deformations are large but the deviations from the equilibrium state are small. In the framework of finite viscoelasticity however, both deformations and deviations from equilibrium are large. In [15], finite viscoelastic constitutive equations have been presented which are based on the multiplicative decomposition of the deformation gradient tensor into elastic and viscous parts. The strain energy function is given by the sum of equilibrium and nonequilibrium parts from which the corresponding stresses are derived. These finite viscoelastic constitutive equations can be easily generalized to incorporate an strain energy limiter. This can be performed by implementing the approach shown in Eq. 14 to enhance the equilibrium part of the strain energy function.

In [1], the HFGMC micromechanical analysis has been derived to establish the behavior of composites in which the constituents are modeled by a finite linear thermoviscoelasticity theory. In [3] and [4] on the other hand, finite viscoelasticity theories have been adopted to represent the viscoelastic and thermoviscoelastic phases of the composite, respectively. In both these two articles, progressive damage has been included in the framework of continuum damage mechanics. Alternatively, these HFGMC micromechanical analyses can be enhanced by incorporating the strain energy limiter concept for the prediction of the composite deformations and failure stresses.

**Acknowledgments** The second author appreciates the support of the Israel Science Foundation (grant No. 394/20).

## References

1. Aboudi, J.: Micromechanics-based thermoviscoelastic constitutive equations for rubber-like matrix composites at finite strains. *Int. J. Solids Struct.* **41**, 5611–5629 (2004)
2. Aboudi, J.: Finite strain micromechanical analysis of rubber-like matrix composites incorporating the Mullins damage effect. *Int. J. Damage Mech.* **18**, 5–29 (2009)
3. Aboudi, J.: Micromechanical modeling of viscoelastic behavior of polymer matrix composites undergoing large deformations. In: Guedes, R.M. (ed.) *Creep and fatigue of polymer matrix composites*, pp. 302–324. Woodhead Pub. Ltd., Oxford (2011a)
4. Aboudi, J.: Finite strain micromechanical modeling of thermoviscoelastic matrix composites. *J. Mech. Mater. Struct.* **6**, 7–29 (2011b)
5. Aboudi, J., Arnold, S.M., Bednarczyk, B.A.: *Micromechanics of composite materials: a generalized multiscale analysis approach*. Elsevier, Oxford (2013)
6. Aboudi, J., Volokh, K.Y.: Failure prediction of unidirectional composites undergoing large deformations. *J. Appl. Mech.* **82**, 071004-1-15 (2015)
7. Aranda-Iglesias, D., Vadillo, G., Rodriguez-Martinez, J.A., Volokh, K.Y.: Modeling deformations and failure of elastomers at high strain rates. *Mech. Mater.* **104**, 85–92 (2017)
8. Christensen, R.M.: *Theory of viscoelasticity*. Academic Press, New York (1982)
9. Hamdi, A., Nait Abdelaziz, M., Ait Hocine, N., Heuillet, P., Benseddiq, N.: A fracture criterion of rubber-like materials under plane stress conditions. *Polym. Test.* **25**, 994–1005 (2006)
10. Holzappel, G.A.: *Nonlinear solid mechanics*. Wiley, New York (2000)
11. Humphrey, J.D.: *Cardiovascular solid mechanics*. Springer, New York (2002)
12. Malvern, L.E.: *Introduction to the mechanics of continuous medium*. Prentice-Hall, Englewood-Cliff (1969)
13. Lockett, F.J.: *Nonlinear viscoelastic solids*. Academic Press, New York (1972)
14. Simo, J.C.: On a fully three-dimensional finite-strain viscoelastic damage model: reformulation and computational aspects. *Comput. Meth. Appl. Mech. Eng.* **60**, 153–173 (1987)
15. Reese, S., Govindjee, S.: A theory of finite viscoelasticity and numerical aspects. *Int. J. Solids Struct.* **35**, 3455–3482 (1998)
16. Simo, J.C., Hughes, T.J.R.: *Computational elasticity*. Springer, New York (1998)
17. Volokh, K.Y.: On modeling failure of rubber-like materials. *Mech. Res. Comm.* **37**, 684–689 (2010a)
18. Volokh, K.Y.: Comparison of biomechanical failure criteria for abdominal aortic aneurysm. *J. Biomech.* **43**, 2032–2034 (2010b)
19. Volokh, K.Y.: Review of the energy limiters approach to modeling failure of rubber. *Rubber Chem. Tech.* **86**, 470–487 (2013)
20. Volokh, K.Y.: On irreversibility and dissipation in hyperelasticity with softening. *J. Appl. Mech.* **81**, 074501-1 (2014)
21. Volokh, K.Y.: *Mechanics of Soft Materials*, 2nd edn. Springer, Berlin (2019)
22. Yeoh, O.H.: Characterization of elastic properties of carbon black filled rubber vulcanizates. *Rubber Chem. Tech.* **63**, 792–805 (1990)

**Publisher's note** Springer Nature remains neutral with regard to jurisdictional claims in published maps and institutional affiliations.